UNIVERSITÄT AUGSBURG
Universitätsbibliothek

OPEN ACCESS
OPUS AUGSBURG

Effect of local wall clearance on scrape-off layer electron density profiles in ASDEX Upgrade

B. Tal, E. Wolfrum, M. Bernert, Gregor Birkenmeier, D. Brida, R. Fischer, G. Grenfell, M. Griener, O. Grover, J. Hobirk, B. Kurzan, T. Lunt, P. A. Schneider, N. Vianello, D. Wendler

Angaben zur Veröffentlichung / Publication details:

Tal, B., E. Wolfrum, M. Bernert, Gregor Birkenmeier, D. Brida, R. Fischer, G. Grenfell, et al. 2024. "Effect of local wall clearance on scrape-off layer electron density profiles in ASDEX Upgrade." *Nuclear Fusion* 64 (12): 126063. https://doi.org/10.1088/1741-4326/ad8362.

Nutzungsbedingungen / Terms of use:

CC BY 4.0

Dieses Dokument wird unter folgenden Bedingungen zur Verfügung gestellt: / This document is made available under these conditions:
CC-BY 4.0: Creative Commons: Namensnennung
Weitere Informationen finden Sie unter: / For more information see:
https://creativecommons.org/licenses/by/4.0/deed.de

nuclear fusion
IAEA

PAPER • OPEN ACCESS

Effect of local wall clearance on scrape-off layer electron density profiles in ASDEX Upgrade

To cite this article: B. Tal *et al* 2024 *Nucl. Fusion* **64** 126063

View the article online for updates and enhancements.

You may also like

- Characterization of the density profile collapse of type I ELMs in ASDEX Upgrade with high temporal and spatial resolution reflectometry
I. Nunes, G.D. Conway, A. Loarte et al.
- Interpretation of fast measurements of plasma potential, temperature and density in SOL of ASDEX Upgrade
J. Horacek, J. Adamek, H.W. Müller et al.
- Large probes in Tokamak scrape-off plasmas. The collisionless scrape-off layer: operation in the shadow of limiters or divertor plates
P C Stangeby

This content was downloaded from IP address 137.250.102.76 on 16/10/2026 at 09:28

OPEN ACCESS
IOP Publishing | International Atomic Energy Agency
Nuclear Fusion
Nucl. Fusion **64** (2024) 126063 (19pp)
https://doi.org/10.1088/1741-4326/ad8362

Effect of local wall clearance on scrape-off layer electron density profiles in ASDEX Upgrade

B. Tal[1], E. Wolfrum[1,*], M. Bernert[1], G. Birkenmeier[1,2], D. Brida[1], R. Fischer[1], G. Grenfell[1], M. Griener[1], O. Grover[1], J. Hobirk[1], B. Kurzan[1], T. Lunt[1], P.A. Schneider[1], N. Vianello[3], D. Wendler[1], the ASDEX Upgrade Team[a] and the EUROfusion Tokamak Exploitation Team[b]

[1] Max-Planck-Institut für Plasmaphysik, Boltzmannstraße 2, 85748 Garching, Germany
[2] TUM School of Natural Sciences, Physics Department, Technical University of Munich, 85748 Garching, Germany
[3] Consorzio RFX, Corso Stati Uniti 4, 35127 Padova, Italy

E-mail: Elisabeth.Wolfrum@ipp.mpg.de

Received 16 May 2024, revised 4 September 2024
Accepted for publication 4 October 2024
Published 25 October 2024

Abstract

The plasma electron density is measured with multiple diagnostics in the scrape-off layer of the ASDEX Upgrade tokamak. The recorded values are typically in good agreement in the case of exponentially decaying profiles at low densities, but they become inconsistent as soon as a density shoulder is formed, and up to a factor of 3 deviation is experienced at high densities. An idea is put forward; namely, that the local plasma-wall proximity has an influence on the local density and thus the measurement results depend on the local limiter-plasma and limiter-diagnostic distances at the same time. The effect of local wall clearance dependence is demonstrated by creating a plasma having an extremely high scrape-off layer density $\left(n_e > 3 \cdot 10^{19}\,\mathrm{m}^{-3}\right)$ after the H-L back transition and varying the position of the separatrix in different directions. As a possible physical process, neutral recycling at the plasma facing components is identified. Similar behaviour is also observed in the QCE regime, where the appearance of small ELMs barely impacts the scrape-off layer profiles. There are also indications that the local wall clearance does have an impact on the density profile not only in the scrape-off layer, but also in the confined region.

[a] See Zohm *et al* 2024 (https://doi.org/10.1088/1741-4326/ad249d) for the ASDEX Upgrade Team.
[b] See Joffrin *et al* 2024 (https://doi.org/10.1088/1741-4326/ad2be4) for the EUROfusion Tokamak Exploitation Team.
[*] Author to whom any correspondence should be addressed.

Original Content from this work may be used under the terms of the Creative Commons Attribution 4.0 licence. Any further distribution of this work must maintain attribution to the author(s) and the title of the work, journal citation and DOI.

Keywords: wall clearance, scrape-off layer, recycling, density profiles, plasma edge

(Some figures may appear in colour only in the online journal)

1. Introduction

One of the major questions concerning magnetically confined fusion is the life cycle of the first wall elements of a reactor. In addition to the mechanical stresses caused by the heat loads, the continuous particle bombardment will erode the material of the plasma facing components. The sputtering yield is governed by the local plasma parameters in front of the wall, including electron density (n_e), the level of which can reach $n_e \approx 4-5\cdot 10^{19}\,\mathrm{m}^{-3}$ in a tungsten (W) wall tokamak when the density limit is approached [1].

It is still under intensive investigation which physical processes determine n_e close to the main chamber wall. As a common observation, n_e increases nonlinearly in the SOL as core n_e is increased [2–10]: the shape of the profiles changes from simple exponentially decaying to flat ones. The amplitude of this density shoulder is defined in many ways depending on the actual profile shape and on the capability of the applied diagnostic in the specific machine. The transition may be controlled by parameters, which are calculated from measurable quantities, although it is not clear which ones: core Greenwald fraction f^{c}_{GW} [4, 11], edge Greenwald fraction f^{e}_{GW} [12], near-SOL divertor collisionality Λ^{near}_{div} [13], fuelling gas flow, i.e. electron flow rate Γ_e [14], turbulence control parameter α_t [15, 16], divertor recycling measured by total divertor H^{div}_{α} [9], main chamber recycling [17].

The investigations of the transition at high n_e typically exploit the capability of one reference diagnostic that can measure in a wide n_e range in the SOL-edge. Only a few efforts have been made to show whether the available systems provide consistent n_e values [5, 7, 10, 18] and generally excellent agreement has been demonstrated.

In this article we go into the details of the latter issue. As a general observation in ASDEX Upgrade discrepancies appear among the n_e levels provided by the different diagnostics in the far SOL when the density shoulder is formed. By further increasing the density the deviations can reach a factor of 3. Based on this inconsistency among a set of available diagnostics, a theory is put forward, namely that the deviations at high n_e are caused by the local proximity of the wall to the plasma. Hence, enhancement in n_e is observed when both the separatrix and the measurement system are close to the limiter. A recent numerical study [19] comparing 2D and 3D SOL simulations with EMC3-EIRENE showed that already at low densities (the separatrix density was matched at about $8\cdot 10^{18}\,\mathrm{m}^{-3}$) the local neutral densities vary considerably depending on whether 2D or 3D structures were taken at the boundary. Further numerical studies at higher densities are subject of future work.

The article is structured as follows: after the introduction of the exploited SOL n_e diagnostics in section 2 their consistent behaviour at low n_e and the inconsistency among them at high n_e is discussed in section 3. An experimental study is introduced in section 4 to show the effect of change in separatrix-wall distance on the n_e measurements. Interpretation, neutral recycling at the plasma facing components as possible physical process and further effects are discussed in section 5. A short summary is given at the end in section 6.

2. Diagnostics

ASDEX Upgrade is equipped with multiple measurement systems that are suitable to determine n_e in the SOL. The poloidal locations of the exploited diagnostics are depicted in figure 1.

The diagnostic typically regarded as the reference for SOL and edge n_e profile measurements is the Lithium Beam Emission Spectroscopy (LiBES) [20]. The system measures on the low field side (LFS) approximately $20-30\,\mathrm{cm}$ above the midplane depending on the plasma position. It is denoted by a brown line in figure 1. Its operation principle is as follows: lithium (Li) ions are extracted from a hot emitter, accelerated with $U \approx 30-50\,\mathrm{kV}$ voltage, neutralized through sodium vapour and injected into the vacuum chamber. Due to the plasma-Li interaction, light is emitted at $\lambda \approx 671\,\mathrm{nm}$, the radial distribution of which is imaged with an optical head looking from the top and with another one looking from the side. The light is then coupled to optical fibers and transmitted to a laboratory, where it is recorded through interference filters with photomultipliers (PMTs) having $f_s = 200\,\mathrm{kHz}$ sampling frequency. n_e is then calculated with a Bayesian code based on a collisional-radiative forward model with weak monotonicity and minimal curvature constraints [21]. As output not only n_e but the corresponding Li_{2p} profiles are provided. These are the smoothest and less curved Li_{2p} profiles which deviate from the raw data only by the measurement errors and called 'measured' light profiles in this study. The program also estimates the profile errors assuming that the perturbing structures are at least 1 cm wide radially. The uncertainties depend also nonlinearly on the time resolution of the reconstruction, which is selected to be a relatively long $(10\,\mathrm{ms})$ value here. This results in averages over small events like filaments and small ELMs and is advantageous in regimes where type I ELMs are not present. The data is only taken from the upper observation system in this investigation, except for the low n_e scans in section 3, where the data of the two optical heads are combined.

The midplane manipulator (MEM) is situated approximately at the same poloidal position and denoted by green in figure 1. It can measure local plasma parameters during the 300 ms long immersion. The high heatflux probehead [22] was used in this study. It is equipped with Langmuir probes (LPs) in Mach arrangement. In this manner the effect of parallel flows, which could significantly bias the n_e estimation

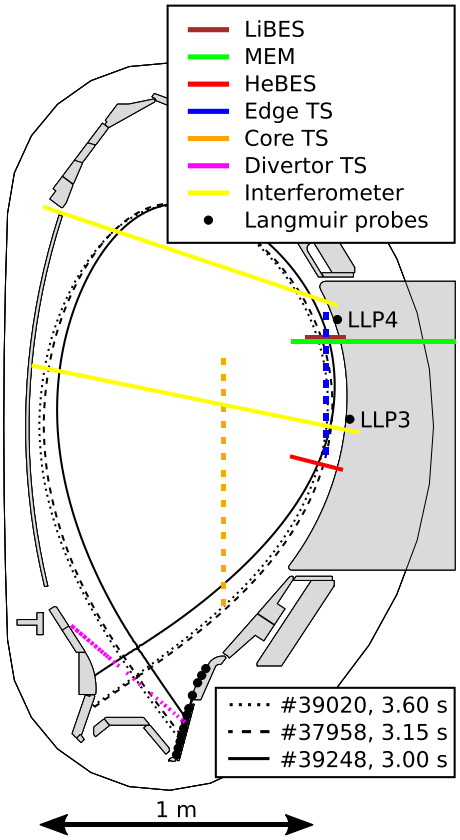


Figure 1. Poloidal locations of the applied electron density diagnostics in the ASDEX Upgrade tokamak. Separatrices of plasmas studied in section 3 are overlaid with thin black lines having different linestyles.

from a single probe measurement, was taken into account and thus a more precise n_e estimation was obtained. Ion saturation currents were measured, T_e profiles were taken from the edge Thomson Scattering (TS) diagnostic and $T_i/T_e = 1.5$ was assumed to deduce n_e.

Helium Beam Emission Spectroscopy (HeBES) [23] is a relatively new diagnostic, the interpretation of which is still intensively studied [24–28]. A piezo valve [29] injects a small amount of helium gas into the plasma SOL. This cloud is observed with radially distributed chords looking nearly tangentially to the field lines. The light is coupled into optical fibers and is transmitted to an optical laboratory. It is decomposed there into 4 colours with interference filters and the intensities of the different wavelengths are recorded with PMTs at $f_s = 900$ kHz sampling frequency. From the ratio of the relatively calibrated line intensities n_e and T_e are determined locally with 1.8 kHz temporal resolution based on the rate coefficients of He [24]. This process is called lookup table method. As measurement locations the shifted centers of the chords are used in the vertical plane of the He beam. The shift is the width of one field of view (3 mm) outward. This way the effect of the finite He cloud width, which weights the light collection volumes outward, is taken into account.

ASDEX Upgrade is equipped with 3 TS diagnostics. In the case of the edge diagnostic [30] pulsed laser light is injected vertically from the bottom at around the outer midplane radius. The light scattered on the plasma electrons is observed with 11 vertically distributed channels having 2.5 cm vertical extension. Unfortunately, the small scattering angles in the case of the lowermost two SOL channels make the signals very noisy there. Hence, they are excluded from the current analysis. The 6 Nd:YAG lasers can fire with 20 Hz repetition rate each. The different beams are slightly shifted horizontally, this way the spatial resolution is enhanced. n_e, T_e and their σ error levels are determined with fits on time dependent signals originating from four polychromator channels in each laser pulse in each observation chord [31]. Spatiotemporal averages are then determined by weighting the individual points by the reciprocals of their variances $1/\sigma^2$. As error levels the weighted standard deviations of each individual point and not of the averages are considered in this article, since the scatter originates not only from statistical uncertainties of the measurement but it is also related to the fluctuations in the measurement quantities. An additional uncertainty is superimposed on the n_e values: the absolute calibration of the six lasers is done with Raman scattering by nitrogen only once or twice in each campaign. With time between these calibrations the laser beam profile shapes are changing, and with this the signal amplitudes observed with the detectors. To compensate for this effect a so called modulo correction is applied on the n_e profiles: an additional relative calibration factor is determined for each laser on a shot-to-shot basis to come to a common mtanh shaped electron density profile in the edge region [32]. Hence, the absolute values of n_e from the TS diagnostic are less reliable than from the 3 diagnostics introduced above. As measurement locations the middle points of the observation chords are considered. They are mapped to the common radial coordinate ρ_p with the IDE equilibrium [33]. This poloidal flux label is $\rho_p = \sqrt{(\Psi - \Psi_{ax})/(\Psi_{sep} - \Psi_{ax})}$, where Ψ, Ψ_{ax} and Ψ_{sep} are the poloidal fluxes at the considered location, at the magnetic axis and at the separatrix [34]. Due to the observation chord distribution the location of gradients in the profiles is highly sensitive to the radial channel positions and to the equilibrium. Hence, the radial chord coordinates are typically shifted with an arbitrary constant value in the evaluation program to get profile positions consistent with the 2-point model [35] and with each other [36]. 3 mm is selected for this purpose below, but accurate location of the gradients does not play a major role in the current investigation. As position (horizontal) error the vertical extension of the channels is considered.

The core TS diagnostic [30] is similar to the edge one: a vertical laser path consisting of 4 laser beams is placed halfway between the outer separatrix and the magnetic axis. The lasers have a repetition frequency of 20 Hz. 16 detectors observe this path at the lower part of the plasma, as shown in figure 1 with orange. n_e, T_e and ρ_p are determined similarly to the method applied to the edge TS. The lowermost 1-2 observation channels are typically in the edge. However, the plasma was shifted up several times in this study and thus these chords

reached the SOL. Considering the 2-point model they could not be regarded then as midplane ones due to the X-point proximity. Since the system is not optimized for low T_e the measurement data was very noisy in these cases. However, reasonable signals were obtained with a rolling 100 ms long median filter if type I ELMs were not present and the plasma parameters changed more slowly than this timescale. There is an unidentified error in the mapping of the radial positions of the system [36]. This is corrected during the evaluation by decreasing the measurement radius by 3 cm. This way the profiles are shifted so that $T_e^{sep} \approx 50\,eV$ is typically obtained at the separatrix in L-mode discharges.

The divertor TS diagnostic is one of the newest systems on ASDEX Upgrade. Its laser obliquely crosses the divertor, as depicted with magenta in figure 1. Only 1 laser is currently available here, which restricts the temporal resolution to 20 Hz. The high field side (HFS) observation chords of the diagnostic are close to each other along the field lines when local plasma parameters are considered. Hence, they are simply labelled by ρ_p. However, due to the uncommon geometry the parallel plasma dynamics is important around the LFS channel locations [37] and thus they cannot be characterized by a simple radial coordinate.

ASDEX Upgrade is equipped with an extensive set of fixed LPs, part of them used in this study is shown with black dots in figure 1. The flush mounted triple probes can provide n_e profiles with $f_s = 22.2\,kHz$. They are installed on the LFS divertor plates and on the so-called transition modules directly above, where the diverted field lines typically end for flux surfaces with flux label $\rho_p > 1.03$. The divertor plates are also equipped with dome-shaped swept probes and the transition modules with flush-mounted swept probes. They can provide n_e values with 800 Hz frequency. To get target profiles these measurements are combined and the temporal resolution is reduced to 50 Hz: the time traces are divided into 20 ms long time periods and their medians are calculated. The graphs containing fixed LP data in this article show the double of the measured density values ($n_e = 2 \cdot n_e^{LPmeas}$ and $p_e = 2 \cdot n_e^{LPmeas} \cdot T_e^{LPmeas}$) to compensate for the presheath acceleration in the 2-point model [35]. Two limiter LPs were also recommissioned for this study: one slightly below the midplane (LLP3) and the other one is on the upper part of the limiter (LLP4). They are single flush-mounted probes with 4 kHz sweeping frequency. They are not placed on the main ICRH antennae limiters, but on the guard limiters, which are retracted by 2 cm [38]. Due to the uncertainties in their effective parallel surfaces the absolute n_e values obtained from these probes are unreliable, but they are suitable to demonstrate temporal changes in n_e.

The standard technique to monitor main plasma n_e is the DCN interferometer [39]. It consists of five channels, two of which are depicted in figure 1 with yellow. The line averaged n_e provided by these chords is used to determine the core Greenwald fraction f_{GW}^c [40] and the edge one f_{GW}^e [12].

The plasma equilibrium is calculated with the IDE [33] equilibrium reconstruction code. It takes all the applicable diagnostics into account in a Bayesian way, where the forward model consists of a Grad-Shafranov solver coupled to the current diffusion equation. Edge pressure gradients and SOL currents are taken into account.

A complex visible light surveillance system monitors plasma-wall interaction during plasma discharges. A fast visible camera looking tangentially and having a wide field-of-view [41] is exploited in this study. It was used in combination with an H_α filter to measure limiter recycling.

3. Deviations in measured SOL density levels in the presence of a density shoulder

The LiBES had been typically used in the earlier density shoulder studies as the reference profile measurement [7, 11–14, 42]. Since it is approximately at the same poloidal location as the MEM is, their consistency is studied first. A simple L-mode discharge #39020 ($I_p = 0.8\,MA$, $B_t = -2.5\,T$, $P_{ECRH} = 0.2\,MW$, $P_{NBI} = 0\,MW$) was formed and its density was ramped up from $n_e = 1.6 \cdot 10^{19}\,m^{-3}$ to $n_e = 3.6 \cdot 10^{19}\,m^{-3}$ by increasing the gas injection rate from the divertor during a 4.4 s long period. This was carried out by density feedback control, where the system varied the electron flow rate in the $\Gamma_e^{div} = 0 - 0.4 \cdot 10^{22}\,s^{-1}$ range. The separatrix position of the discharge is shown in figure 1 with a dotted black line, the SOL was limited by the HFS heat shield. Four successful MEM plunges were carried out during the ramp up [22]. The results are shown in figure 2 with dashed lines. The corresponding n_e levels in f_{GW}^e units are written in the legend. The LiBES profiles are averaged over 400 ms long periods around the plunges and shown with solid lines and corresponding colours. Additionally, solid vertical lines denote the nearly constant (HFS) limiter positions. The good agreement between the profiles in the outer SOL demonstrates that no toroidal asymmetry is observed when the profiles decay exponentially. (In this discharge type the flattening would have taken place when $f_{GW}^e > 0.3$ [12].)

The consistency between the LiBES and the HeBES profiles at low n_e has already been demonstrated in some simple cases [24, 25]. It is corroborated here with a highly N_2-seeded density ramp up discharge #37958 ($I_p = 1\,MA$, $B_t = -2.5\,T$, $P_{ECRH} = 0.8\,MW$, $P_{NBI} = 0\,MW$). The D_2 electron flow rate was controlled in this case: it was increased from $\Gamma_{e,D_2}^{div} = 0.2 \cdot 10^{22}\,s^{-1}$ to $\Gamma_{e,D_2}^{div} = 10^{22}\,s^{-1}$ and the electron flow rate of the seeding gas was kept constant $\Gamma_{e,N_2}^{div} = 0.56 \cdot 10^{22}\,s^{-1}$. In this manner the $n_e = 3.1 \cdot 10^{19}\,m^{-3} - 6.2 \cdot 10^{19}\,m^{-3}$ density range was spanned. The separatrix position of the discharge is shown in figure 1 with a dashed black line, the SOL was limited by the HFS heat shield here, too. The profiles are shown in figure 3. The ramp up is divided into 5 n_e ranges, the profiles are averaged over them and shown with corresponding colours. The agreement between the two diagnostics was very good in the $\rho_p = 1.01 - 1.035$ spatial range, especially when $f_{GW}^e < 0.3$, i.e. below the n_e shoulder formation threshold. The slight deviation in the outer HeBES measurement locations can be explained by diagnostic issues: the He gas is not in

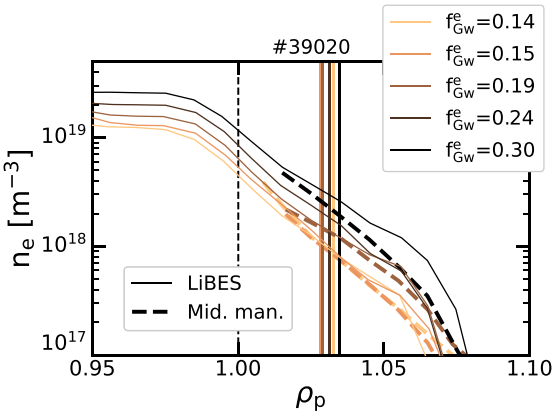


Figure 2. Comparison of electron density profiles in the SOL measured with the MEM (dashed lines) and with the LiBES (solid lines) in the density ramp up discharge #39020. Colour coding depicts the different time periods and thus n_e and Greenwald fraction levels. Solid vertical lines: closest (HFS) limiter locations, dashed vertical black line: separatrix position.

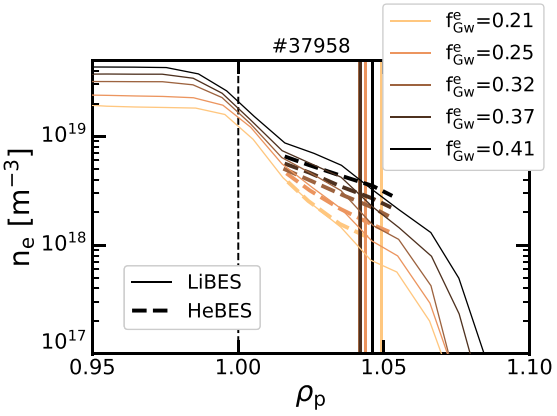


Figure 3. Comparison of electron density profiles in the SOL measured with the HeBES (dashed lines) and with the LiBES (solid lines) in the N_2 seeded density ramp up discharge #37958. Colour coding depicts the different time periods and thus n_e and Greenwald fraction levels. Solid vertical lines: closest (HFS) limiter locations, dashed vertical black line: separatrix position.

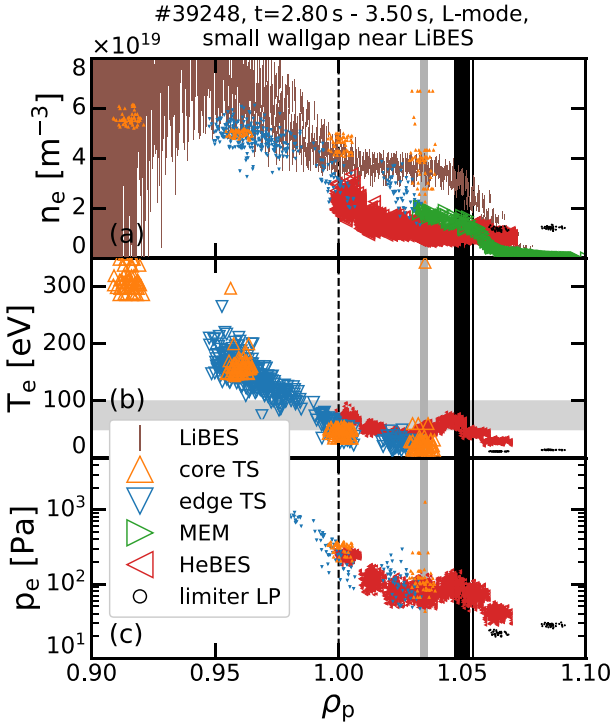


Figure 4. Electron density (*a*) and temperature (*b*) profiles in linear scale and pressure (*c*) profiles in logarithmic scale in the SOL measured with various diagnostics in #39248. The vertical extensions of the brown lines denote the profile and estimation uncertainties of the LiBES. Simple data points are plotted for the other diagnostics with large symbols if they are regarded reliable. Small symbols are used if the data are considered less reliable. Vertical grey lines: end of outer divertor, vertical solid black lines: location of the limiter, dashed vertical black lines: separatrix position. For poloidal locations of the diagnostics and separatrix position see figure 1. Horizontal grey patch in (*b*): $T_e = 50\,\mathrm{eV} - 100\,\mathrm{eV}$ range, i.e. the possible range of the upstream separatrix temperature.

the assumed thermal equilibrium there and the lookup table method does not deal with reabsorption, which may not be negligible in this region [25].

A deviation up to a factor of 3 among the three diagnostics is found at high $n_e \approx 7 \cdot 10^{19}\,\mathrm{m}^{-3}$ (and thus relatively high $f^e_{GW} \approx 0.65$) with developed density shoulder. In order to create these conditions an H-mode discharge was formed at first with very low gas injection rate and with moderate auxiliary heating power: $P_{ECRH} = 2.3\,\mathrm{MW}$ and $P_{NBI} = 2 - 2.5\,\mathrm{MW}$ (one NBI source with full power). Then an H-L back transition was initiated by increasing the gas fuelling only from the divertor to the maximum available level of $\Gamma_e^{div} \approx 10^{23}\,\mathrm{s}^{-1}$ and instantaneously switching off the ECRH heating. #39341, #41386 and #39248 belong to this discharge type in this article, they are introduced in detail in section 4.1 and in section 4.3. These plasmas were limited at the top part of the ICRH limiter on the LFS near the LiBES. The discrepancy was the highest when the plasma was pushed close to this limiter, like in the $t = 2.8\,\mathrm{s} - 3.5\,\mathrm{s}$ timerange of #39248. (Although the wall clearance was still 4 cm.) The corresponding separatrix geometry is shown with a solid thin black line in figure 1. The n_e and additionally the T_e and p_e profiles are depicted in figure 4. Here a bunch of black vertical lines denotes the positions of the limiter. Additionally, the location of the flux surface, where the outer divertor ends and the divertor plates start to bend out, is also shown by vertical grey lines. One can conclude that the profiles are flat in the far SOL spreading up to the limiter and all 3 diagnostics measure values in the SOL, which are unusually high and deviate significantly: $n_e^{HeBES} \approx 0.9 \cdot 10^{19}\,\mathrm{m}^{-3}$ (red), $n_e^{MEM} \approx 1.7 \cdot 10^{19}\,\mathrm{m}^{-3}$ (green), $n_e^{LiBES} \approx 3.3 \cdot 10^{19}\,\mathrm{m}^{-3}$ (brown). These values are spatial averages between the grey and black vertical lines. A question arose regarding whether LiBES overestimates n_e in the developed shoulder case, when filamentary transport is significant [7] and thus the profiles are not necessarily monotonic. This possibility is examined numerically in appendix and dismissed. The profiles measured by the TS systems are also shown, although the n_e profiles are considered to be less reliable due to calibration and

X-point proximity issues. Hence, they are depicted with small symbols in figures 4(*a*) and (*c*). The edge TS system indicates that $n_e^{\mathrm{HeBES}} < n_e^{\mathrm{edgeTh}} < n_e^{\mathrm{LiBES}}$ and in case of the core system $n_e^{\mathrm{coreTH}} \approx 1.2 \cdot n_e^{\mathrm{LiBES}}$. The absolute values provided by the limiter LPs are also regarded less reliable due to the uncertainties in the effective parallel surfaces of the probes and in the fits to the LP sweep characteristics. Hence, they are depicted by only small black symbols in the entire figure. Considering T_e the HeBES had some calibration issues, which affected mainly the T_e estimation and thus it is plotted only with small symbols in figures 4(*b*) and (*c*). $T_e^{\mathrm{edgeTh}} = 22.4 \pm 8\,\mathrm{eV}$ was measured at the outermost available edge TS channel.

Before interpreting the results introduced above, the termination of the density shoulder outwards is investigated. It can be observed from figure 4 that the profiles have a very long falloff length in the far SOL up to $\rho_p \approx 1.04 - 1.05$. Outwards of this point n_e decays sharply. The question arose whether the termination point is determined either by the classically defined global limiter location, i.e. by the ρ_p of the deepest immersed solid surface, which can be poloidally very far away from the diagnostic, or by the wall locally close to the diagnostic or by the SOL transport itself, like at JET [9]. This was tested by varying the plasma-wall distance at different locations and measuring the profiles with the LiBES. The results are shown in figure 5, where the limiter location is denoted by solid lines and ρ_p of the wall at the LiBES height is denoted by dash-dotted ones. In the left column the plasma was limited on the top of the ICRH limiter, i.e. close to the LiBES and this clearance was increased from 4 cm to 7.5 cm. The extension of the profiles followed the change, so the location of termination is related to a wall distance. (The change in the n_e plateau height is regarded as an effect of other nature and considered in section 4.3). To test whether the global limiter location is relevant from the termination aspect or the local plasma-wall distance another experiment was carried out and is introduced in the right column: here the plasma was limited at the bottom of the ICRH limiter with a wall clearance of $8 - 9$ cm and the plasma-wall distance at the LiBES height was increased from 6 cm to 10 cm. This change did not have an influence on extension of the shoulder. Hence, one can conclude that the nonlocal location of the limiter determines the shoulder extension in this plasma scenario at ASDEX Upgrade.

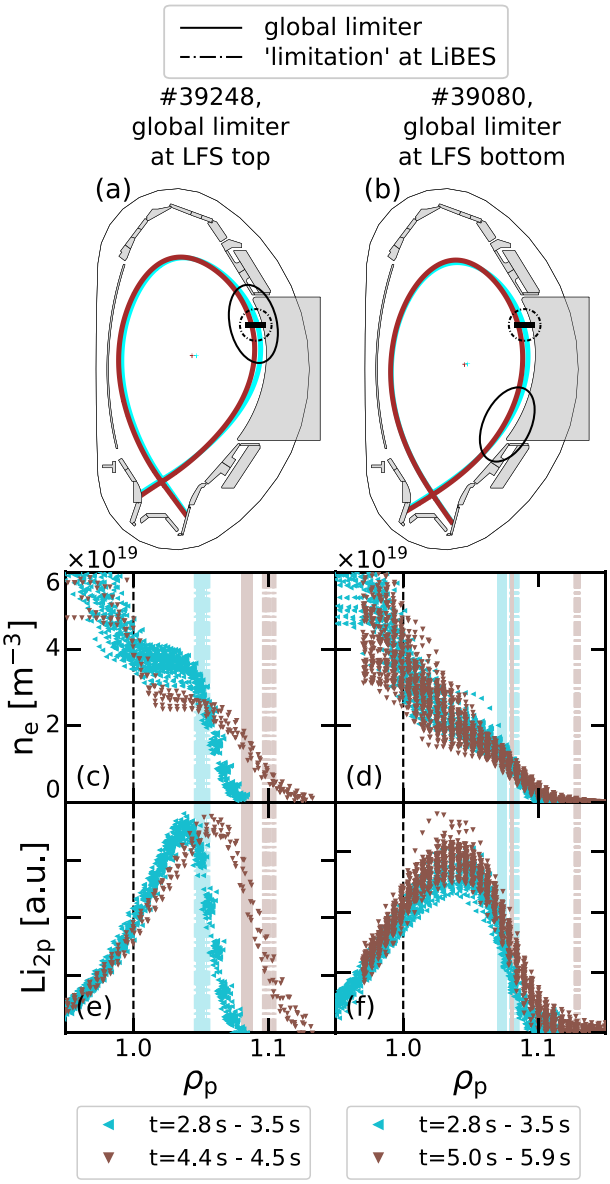


Figure 5. Effect of limiter location on the radial extension of density shoulder measured by the LiBES. Left: #39248 - plasma limited on the LFS top, right: #39080 - plasma limited on the LFS bottom. Cyan: small wall gap, brown: large wall gap. (*a*) and (*b*): AUG geometry, separatrices (colourful lines), LiBES (thick black vertical line) and 'limitation' locations. (*c*) and (*d*): reconstructed n_e. (*e*) and (*f*): measured Li_{2p} profiles. Solid vertical lines: innermost global limiter positions, dash-dotted vertical lines: limitation locations at the LiBES height—they are faded out only for better visibility of the profiles. The corresponding 'limitation' locations are encircled with corresponding linestyles in (*a*) and (*b*). Dashed vertical black lines: separatrix position.

4. Local plasma-wall distance scans

Regarding the question of whether the observed discrepancies at high SOL n_e could come from the local proximity to the wall, two distances should be considered: the absolute (mainly toroidal) limiter-diagnostic and the radial limiter-separatrix distance. Since the first one cannot be changed during a campaign, the second one was varied and the observations are presented in this section.

4.1. Strike point scan in L-mode

One method to increase the local plasma-wall distance is to shift the plasma upward slowly by 7 cm with only minor change in shape. In this manner the bottom part of the plasma moves away from the wall. The scan is referred to as a strike point scan [37]. The separatrix positions before and after this scan are shown in figure 6(*a*) and the basic time traces are depicted in panels (*b*)–(*i*). The radius of the separatrix at the midplane remained constant during the movement, as shown in figure 6(*b*), which also resulted in a nearly constant 5.5 cm plasma-wall distance near the LiBES location. As suggested

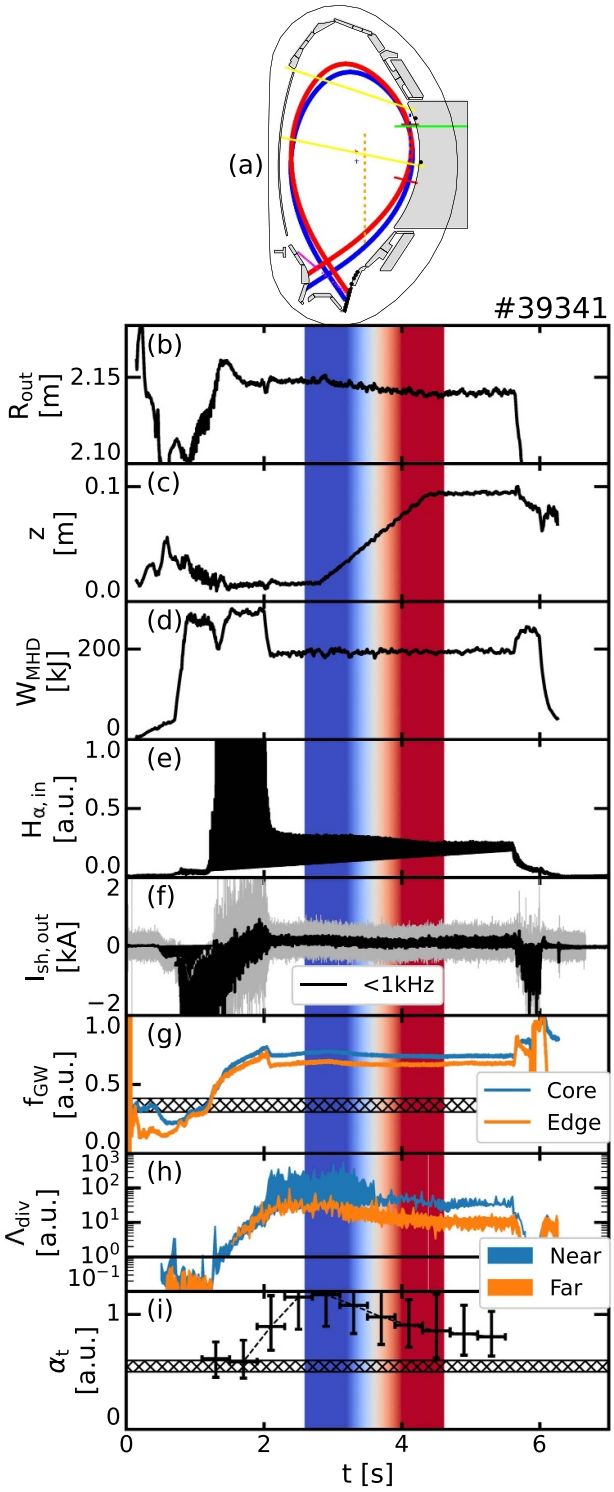


Figure 6. Separatrix positions (*a*) and time traces (*b*)–(*i*) of the L-mode strike point scan #39341. Outer separatrix radius (*b*), plasma axis height (*c*), MHD plasma energy (*d*), total H_α radiation in the inner divertor (*e*), shunt current in the outer divertor (*f*) with 200 kHz sampling frequency (grey) and low-pass filtered to 1 kHz (black), core (blue) and edge (orange) Greenwald fractions (*g*) with shoulder formation threshold denoted by a horizontal hatch, near (blue) and far SOL (orange) divertor collisionalities (*h*) with threshold denoted by a horizontal black line and turbulence parameter (*i*) including its error bars with threshold denoted by a horizontal hatch. Background patch in the $t = 2.6\,\mathrm{s} - 4.6\,\mathrm{s}$ time range colour codes the plasma height in the strike point scan of figure 7, 9 and 20.

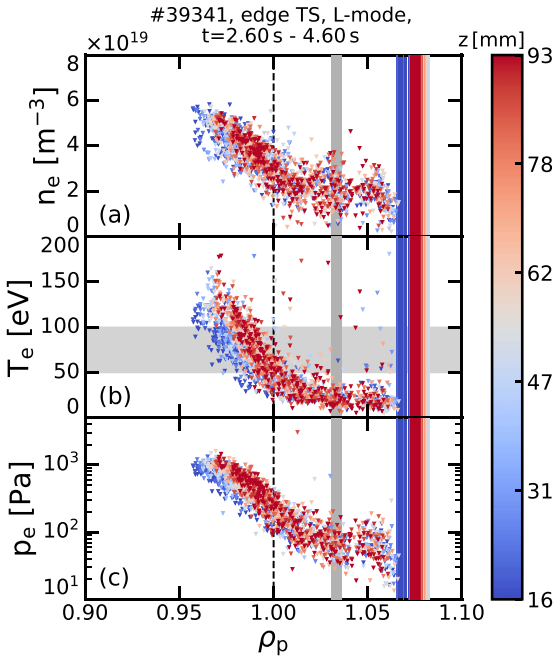


Figure 7. Electron density (*a*), temperature (*b*) and pressure (*c*) profiles around the midplane measured with the edge TS diagnostic during the L-mode strike point scan in #39341. Colour code: plasma axis height. Vertical grey lines: end of outer divertor, colourful vertical lines: limiter positions, dashed vertical black lines: separatrix position. Horizontal grey patch in (*b*): $T_e = 50\,\mathrm{eV} - 100\,\mathrm{eV}$ range, i.e. the possible range of the upstream separatrix temperature.

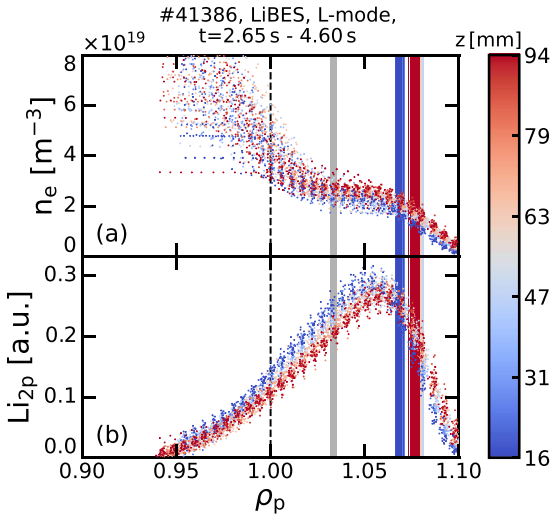


Figure 8. Electron density (*a*) and measured Li_{2p} emission (*b*) based on LiBES measurements around the midplane during the L-mode strike point scan in #41386. Colour code: plasma axis height. Vertical grey lines: end of outer divertor, colourful vertical lines: limiter positions, dashed vertical black lines: separatrix position.

by the Greenwald fraction time traces in (*g*) the scan had negligible impact on the line averaged n_e. It was carried out in the $t = 2.8\,\mathrm{s} - 4.4\,\mathrm{s}$ time range, as shown in (*c*). The patch in the background codes the vertical position of the plasma with colours. This coding is used later in figures 7, 9 and 20.

The considered L-mode discharge #39341 ($I_p = 0.8\,\mathrm{MA}$, $B_t = -2.5\,\mathrm{T}$) was started with a short H-mode phase, when $P_{NBI} = 2.4\,\mathrm{MW}$ and $P_{ECRH} = 2.3\,\mathrm{MW}$ auxiliary heating were used and the gas fuelling was continuously increased to a level of $\Gamma_e^{div} \approx 10^{23}\,\mathrm{s}^{-1}$. This is the maximum level which the divertor fuelling valves of ASDEX Upgrade can deliver. Since it was only marginally enough for an H-L back transition, a small amount of D_2 ($\Gamma_e^{MC} \approx 10^{22}\,\mathrm{s}^{-1}$) was also injected from the main chamber. Then, at $t = 2\,\mathrm{s}$ the ECRH heating was switched off, which initiated an H-L back transition, resulting in the decrease of W_{MHD} (*d*) and f_{GW} (*g*). The ELMs also disappeared, which is illustrated by the reduction of fluctuations in the inner divertor H_α (*e*) and in the outer divertor shunt current (*f*) measurements. As shown in (*g*)–(*i*), the possible density shoulder control parameters indicate that it should be formed: $f_{GW}^e \approx 0.65$, when the transition threshold is at approximately $0.3 - 0.4$ [12], $\Lambda_{div}^{near} \approx 25 - 215$, when the transition threshold is 1 [13], and $\alpha_t > 0.6$ when the transition threshold is at approximately $0.5 - 0.6$ [15]. (The threshold ranges are denoted with horizontal black hatches and a horizontal black line.)

Figure 7 shows the electron profiles measured with the edge TS diagnostic during the scan. The separatrix is denoted by a single dashed black vertical line, the limiter location with solid lines having corresponding colours and the end of the divertor with vertical grey lines. The n_e and T_e profiles have a very long falloff length and they are practically not affected by the scan in the far scrape-off layer, where $n_e = 1 \pm 0.8 \cdot 10^{19}\,\mathrm{m}^{-3}$ and $T_e = 16 \pm 6.9\,\mathrm{eV}$. Although a small change in the T_e gradient location can be observed in this special example in the confined region, other similar discharges do not feature this variation. The n_e profiles remained constant during the entire scan in the confined region.

Technical problems arose in #39341 with the LiBES diagnostic. Hence, profiles from an exact repetition of the discharge are shown in figure 8, where (*a*) depicts the n_e profiles and (*b*) the measured Li_{2p} emission [21]. The minor change in the limiter location slightly varied the termination point of the profiles. This can be noticed, especially in (*b*). Otherwise the profiles are flat and not influenced by the strike point scan, similarly to the edge TS measurements.

The divertor conditions during the strike point scan are summarized in figure 9. The capabilities of the divertor TS system are exploited to characterize the plasma in the inner divertor. The obtained radial profiles, as discussed in section 2, are shown in the left column. The plasma was detached there and the high field side high density region (HFSHD) [43] was always present with increasing n_e from $1.5 \cdot 10^{20}\mathrm{m}^{-3}$ to $3 \cdot 10^{20}\mathrm{m}^{-3}$ as the plasma moved up. The electron temperature was below 2 eV during the entire scan. The profiles in the outer divertor, which were measured with LPs, are shown in the right column of the same figure. As explained in section 2 $n_e = 2 \cdot n_e^{meas}$ and $p_e = 2 \cdot n_e^{meas} T_e^{meas}$ are depicted

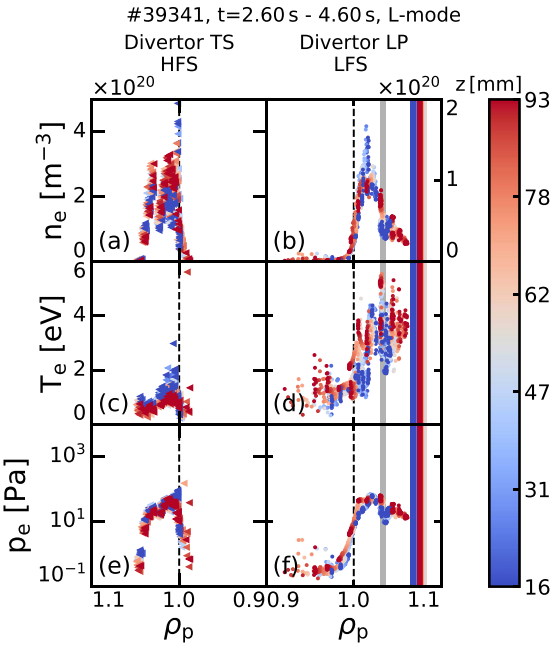


Figure 9. Electron density (*a*)/(*b*), temperature (*c*)/(*d*) and pressure (*e*)/(*f*) profiles measured in the HFS/LFS divertor during the L-mode strike point scan in #39341. Colour code: plasma axis height. Vertical grey lines: end of outer divertor, colourful vertical lines: limiter positions, dashed vertical black lines: separatrix position. Left: HFS, measured with divertor TS, right: LFS, measured with LPs.

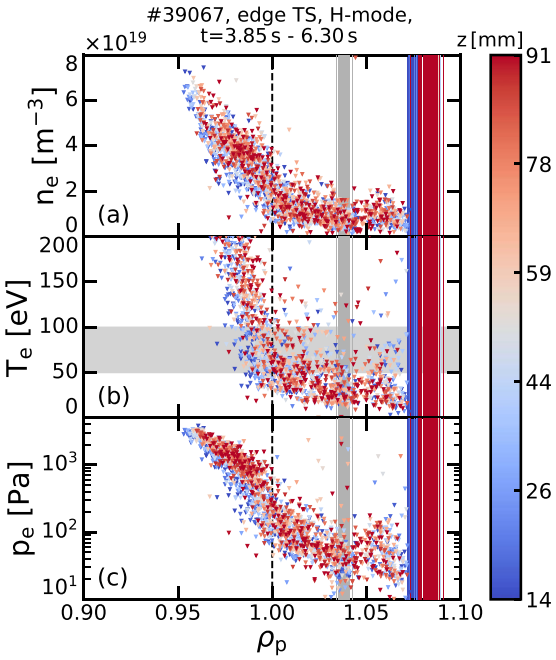


Figure 10. Electron density (*a*), temperature (*b*) and pressure (*c*) profiles around the midplane measured with the edge TS diagnostic during the H-mode strike point scan in #39067. Colour code: plasma axis height. Vertical grey lines: end of outer divertor, colourful vertical lines: limiter positions, dashed vertical black lines: separatrix position. Horizontal grey patch in (*b*): $T_e = 50\,\text{eV} - 100\,\text{eV}$ range, i.e. the possible range of the upstream separatrix temperature.

to compensate for the presheath acceleration effect. The outer divertor plasma was partially detached [44] and the profiles were not influenced by the strike point scan. n_e decreased from $10^{20}\,\text{m}^{-3}$ to $5 \cdot 10^{19}\,\text{m}^{-3}$ outwards, but always remained above the midplane value. T_e was higher here than in the inner divertor, but it stayed below 5 eV during the considered time range. It increased outwards, simultaneously to the decrease of n_e and it always stayed below the midplane value.

In summary, the strike point scan measurements in L-mode with developed density shoulder showed that the profiles were influenced neither at the midplane nor in the outer divertor by the movement.

4.2. Strike point scan in H-mode

An experiment similar to the one introduced in section 4.1, but in H-mode, was carried out in discharge #39067. This was achieved by doubling the auxiliary heating power ($P_{\text{NBI}}^{\text{H-mode}} = 5\,\text{MW}$ was used here compared to the $P_{\text{NBI}}^{\text{L-mode}} = 2.4\,\text{MW}$ in the L-mode discharge) and halving the gas injection rate from the divertor, i.e. only $\Gamma_e^{\text{div,H-mode}} = 4.8 \cdot 10^{22}\,\text{s}$ electron flow rate was applied in H-mode compared to $\Gamma_e^{\text{div,L-mode}} = 10.1 \cdot 10^{22}\,\text{s}^{-1}$ in L-mode. Additionally, the gas inlet at the midplane, which was used to inject fuel with $\Gamma_e^{\text{MP,L-mode}} = 10^{22}\,\text{s}^{-1}$ electron flow rate in L-mode, was also switched off. In this way, the QCE regime [45] was achieved. The edge-SOL plasma was in a dynamic state, where the filaments and small ELMs were not distinguishable from the quiescent periods and therefore included in the profiles. The ELM monitoring measurements suggested that the properties of the events (size, frequency) were influenced by the strike point location. However, it was not clear whether this was caused only by the changing coverage of the measurement relative to the strike point or the plasma conditions indeed changed.

As depicted in figure 10 the edge TS measurements show similar behaviour in H-mode as in L-mode: the profiles were flat in the far SOL and not influenced by the strike point scan, despite the apparently changing ELM activity during the scan. n_e was lower than in the L-mode case and $T_e = 12.8 \pm 12.6\,\text{eV}$ had similar average and higher fluctuation levels compared to L-mode.

Similarly to the earlier observations, the LiBES profiles were only slightly influenced by the scan due to the slightly changing limiter location, as shown in figure 11.

4.3. Plasma-wall distance variation around the midplane

In another experiment (#39248), the local plasma-wall distance was varied around the midplane, i.e. poloidally close to the reference diagnostics. The separatrix positions before and after this change are shown in figure 12(*a*) and the basic time traces are depicted in the panels below.

The initial part of discharge #39248 consisted of a short H-mode phase to ramp the gas injection rate up, similarly to section 4.1. However, the D_2 gas inlet at the midplane was switched off in this case to avoid any possible fuelling location induced asymmetries. Then a fast strike point scan shown

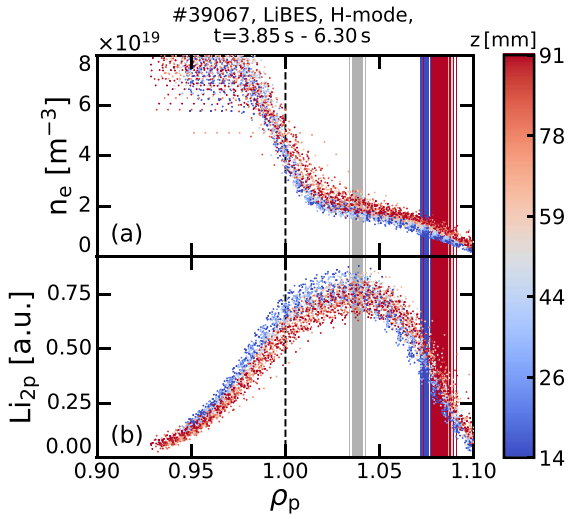


Figure 11. Electron density (*a*) and measured Li_{2p} emission (*b*) based on LiBES measurements around the midplane during the H-mode strike point scan in #39067. Colour code: plasma axis height. Vertical grey lines: end of outer divertor, colourful vertical lines: limiter positions, dashed vertical black lines: separatrix position.

in figure 12(*c*) was done in order to ensure that the SOL is limited by the top part of the ICRH antennae limiter close to the LiBES. In the first stable period $t = 2.8\,\mathrm{s} - 3.5\,\mathrm{s}$ (denoted by a cyan patch in figure 12) the wall clearance was 4 cm at the LiBES height. This was increased to around 7.5 cm, as depicted in (*b*), and a short stationary L-mode phase was achieved: $t = 4.4\,\mathrm{s} - 4.5\,\mathrm{s}$, denoted by a brown vertical bar. This modification did not have an influence on the line averaged n_e, as indicated by the nearly constant value of the Greenwald-fractions in L-mode in (*g*). Then a spontaneous L-H transition occurred, as indicated by the increasing W_{MHD} and f_{GW} in (*d*) and (*g*) and by the increased fluctuation levels in (*e*) and (*f*). This way two stationary phases in the QCE regime were also recorded, denoted by yellow and purple vertical bars. Figure 12(*c*) shows that small amplitude strike point sweeps were also carried out to enhance LP coverage in the divertor. The possible shoulder control parameters f_{GW} and Λ_{div}^{near} were far above the threshold in the discharge, as depicted in (*g*) and (*h*). α_t could be calculated only in the small wall clearance case since the separatrix region was only marginally covered later by the edge TS diagnostic. In this first period $\alpha_t > 0.6$ and there is no indication that it decreased later.

The profiles, provided by the LiBES in the four time ranges, are depicted in figure 13. The marker sizes of the short time periods denoted by brown and yellow are increased here for better visibility. The faded vertical lines show the limiter positions in the corresponding periods. The same profiles from the first two time ranges have already been reported in figure 5, where the termination point was considered. Here another observation is introduced: the proximity to the wall can increase n_e throughout the entire far SOL. In this example the separatrix was much closer to the wall in the case with cyan markers and thus n_e was 30 percent higher in the $\rho_p = 1.02 - 1.05$ range. A similar phenomenon has been demonstrated in TCV, although it was not a local effect there [17]. In AUG the behaviour was experienced in this divertor fuelled experiment and not in the case, when the plasma was fuelled with the top and midplane valves (not shown here). However, this latter observation may have been related to technical problems with the diagnostic and will be subject to future studies. Additionally, it is noted that the L-H transition occurs in the pedestal and it did not have an influence on the n_e levels in the far SOL.

The increased SOL n_e due to reduced wall clearance is corroborated with the help of the upper 4 channels of the edge TS diagnostic shown in figure 14. (As explained in section 2 the lower channels were too noisy for this investigation.) The left and right columns depict the small and high plasma-wall distance cases, respectively. For this comparison the 10 ms long L-mode time range in the high wall clearance case is not long enough. Hence, the entire time range, when the plasma was far away from the wall, is used, including L-mode, H-mode and the small strike point sweep, too. An additional complication is related to the stability of individual lasers in the edge TS system, which can affect the absolute calibration of n_e. To overcome this issue the measurements with only 3 lasers are plotted with different colours and the modulo correction, which was described in section 2, is not applied. As error bars the weighted $1 \cdot \sigma$ values of the individual measurement points are shown with faded colours. Additionally, the error bars of the estimated random scatters of the averages are denoted. They are $1/\sqrt{N}$ times lower than the faded ones, where the number of useful measurement points is $N \approx 20 - 30$. The comparison between the left and right columns suggests elevated n_e in the small wall clearance case. The LiBES measurements are overlaid with brown colour. As it was already shown in figure 13, they also display this trend. Additionally, the edge TS n_e values are systematically lower than the LiBES measurement values, as it was mentioned in section 3.

As a further confirmation, the n_e evolution in the SOL is demonstrated by showing time traces of two limiter LPs in figure 15. Here the basic discharge parameters are repeated in (*a*)–(*c*) and the average of the SOL n_e in the $\rho_p = 1.02 - 1.05$ range measured with the LiBES is shown in (*d*). The calculated n_e signals from the swept guard limiter LPs are shown in (*e*) and in (*f*). The signals, which are highly fluctuating due to filament activity, are shown in grey. The dotted and the solid colourful lines correspond to the lower envelope (0.25 quantile) and mean over 20 ms, respectively [46]. The radial locations are shown in (*g*) with corresponding colours. Here the limiter shadow is hatched and a black nearly horizontal line denotes the end of the divertor. Poloidally the LLPs are close to the zone where the local wall gap was changed, as shown in figure 12(*a*). The measurement signals clearly indicate the enhanced n_e with reduced wall clearance, although their absolute values are not entirely reliable. (*h*) is related to H_α measurements on the limiter and discussed in section 5.

Similarly to the strike point scan, the effect of changing local wall clearance is also investigated at a location far away, namely in the divertor. This is shown in figure 16. The graphs

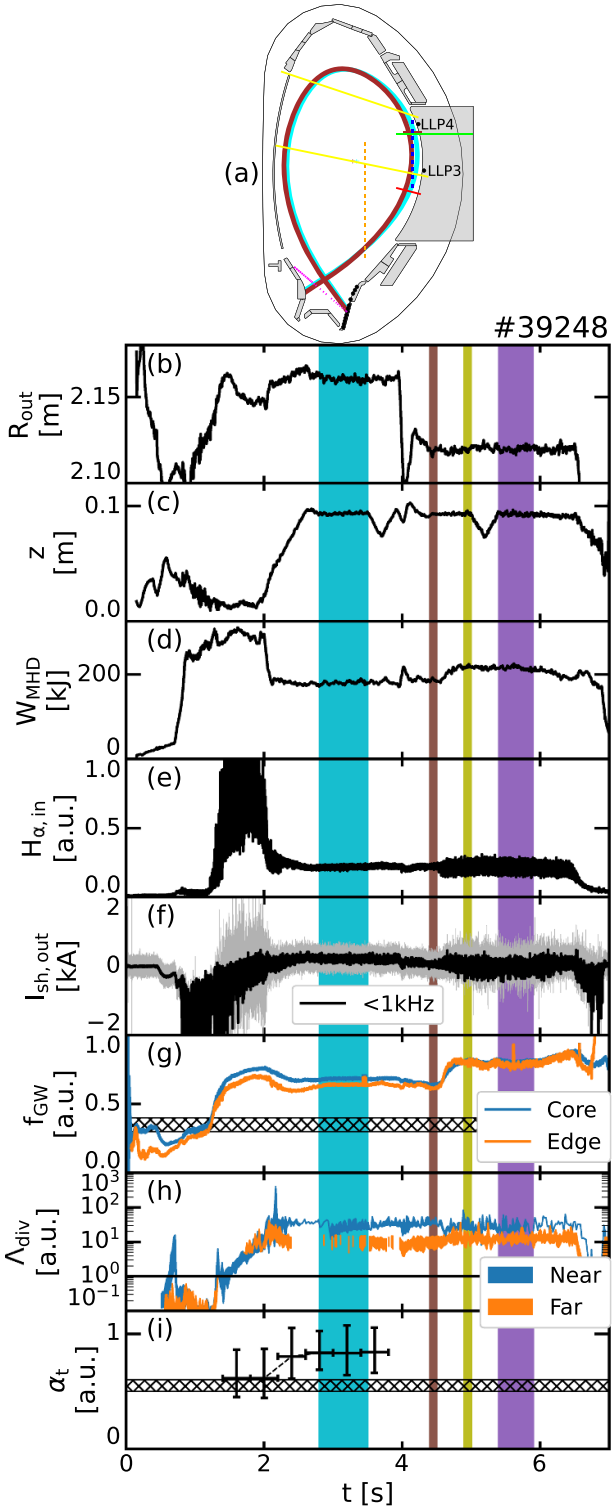


Figure 12. Separatrix positions (*a*) and time traces (*b*)–(*i*) of the outer wall clearance variation discharge #39248. Outer separatrix radius (*b*), plasma axis height (*c*), MHD plasma energy (*d*), total H_α radiation in the inner divertor (*e*), shunt current in the outer divertor (*f*) with 200 kHz sampling frequency (grey) and low-pass filtered to 1 kHz (black), core (blue) and edge (orange) Greenwald fractions (*g*) with shoulder formation threshold denoted by a horizontal hatch, near (blue) and far SOL (orange) divertor collisionalities (*h*) with threshold denoted by a horizontal black line and turbulence parameter (*i*) including its error bars with threshold denoted by a horizontal hatch. Background patches identify time periods used in figure 13, 15–17.

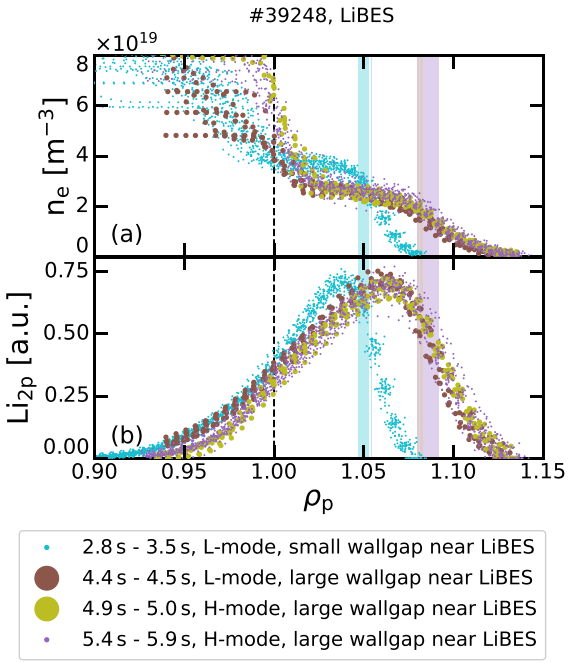


Figure 13. Electron density (*a*) and measured Li_{2p} emission (*b*) based on LiBES measurements around the midplane in the outer wall clearance variation discharge #39248. Time ranges are denoted with corresponding colours in figure 12. Colourful vertical lines: limiter positions, dashed vertical black lines: separatrix position. The vertical lines are faded out for better visibility of the profiles.

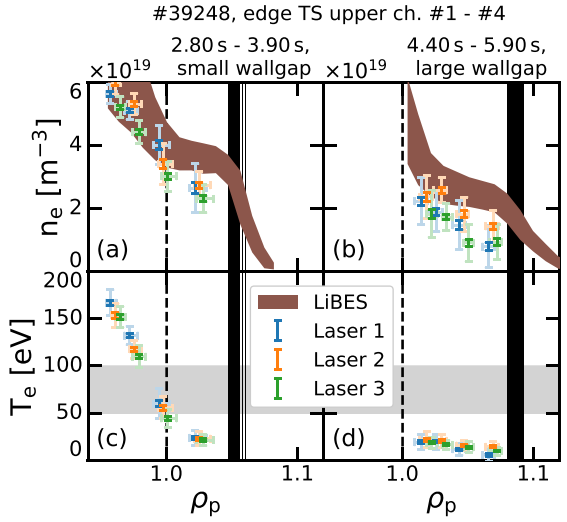


Figure 14. Electron density (*a*), (*b*) and temperature (*c*), (*d*) profiles around the midplane measured with the top 4 channels of the edge TS diagnostic in the outer wall clearance variation discharge #39248. Left column: small wall gap around the LiBES location in L-mode, right column: high wall gap around the LiBES location, where L- and H-mode periods are also included. Different colours denote the different lasers. Faded and colourful vertical error bars: weighted $1 \cdot \sigma$ levels of the individual measurement points and the averages. The typical tanh fit correction on n_e is not used. Brown patch: LiBES measurement confidence range. Solid vertical black lines: location of the limiter, dashed vertical black lines: separatrix position. Horizontal grey patch in the bottom row denotes $T_e = 50\,\text{eV} - 100\,\text{eV}$ range, i.e. the possible range of the upstream separatrix temperature.

are similar here to figure 9: the left column shows the properties of the inner divertor plasma measured by TS diagnostic and the right column the outer one measured with LPs. The two L-mode phases are compared and no difference was observed, as expected.

4.4. Effect of L-H transition on the developed shoulder with high wall clearance

It was demonstrated in figure 13 that the L-H transition and the appearance of small ELMs did not influence the shoulder

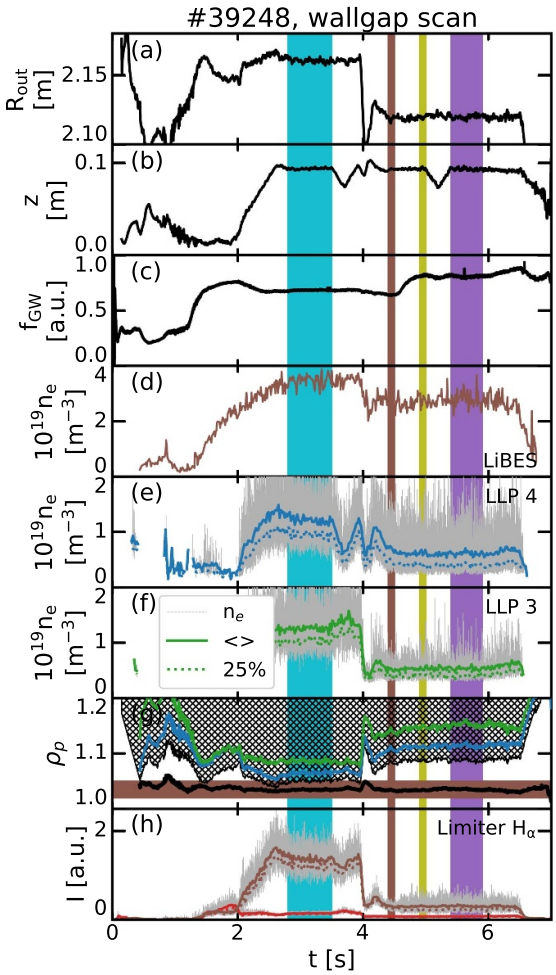


Figure 15. Additional time traces of the outer wall clearance variation discharge #39248. Outer separatrix radius (*a*), plasma axis height (*b*), Greenwald fraction (*c*), electron density measured with LiBES in the $\rho_p = 1.02 - 1.05$ range (*d*) and with limiter Langmuir probe LLP4 (*e*) and LLP3 (*f*). ρ_p of the applied LiBES spatial range, i.e. $\rho_p = 1.02 - 1.05$ (horizontal brown patch) and of the LLPs (blue and green lines) are shown in (*g*), where the limiter shadow is hatched and a black nearly horizontal time trace shows the end of the divertor. For poloidal locations of LLPs see figures 1 and 12(*a*). Background-subtracted limiter H_α radiation is depicted in (*h*), the ROIs of which are shown in figure 18 with corresponding colours. Grey signals are with full available temporal resolution in (*e*), (*f*) and (*h*), solid and dotted colourful signals are downsampled to 20 ms with mean and 0.25 quantile. Colourful vertical background patches denote the time periods already indicated in figure 12.

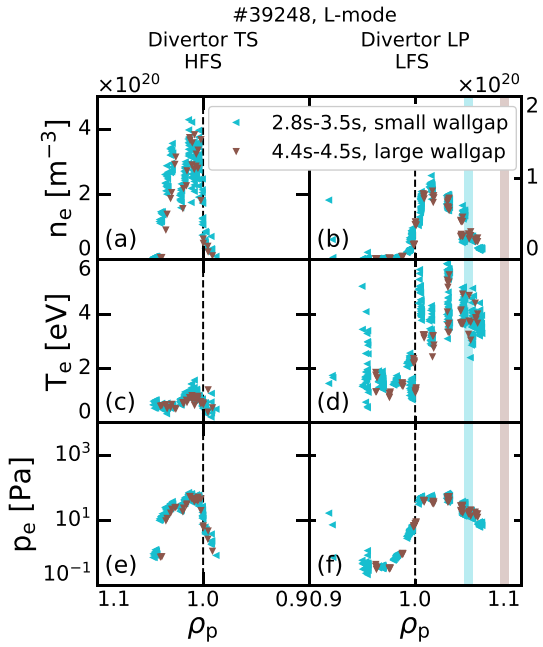


Figure 16. Electron density (*a*)/(*b*), temperature (*c*)/(*d*) and pressure (*e*)/(*f*) profiles measured in the HFS/LFS divertor during the L-mode periods of the outer wall clearance variation discharge #39248. The here applied time ranges are denoted with corresponding colours in figure 12. Colourful vertical lines: limiter positions, dashed vertical black lines: separatrix position. The vertical lines are faded out for better visibility of the profiles. Left: HFS, measured with divertor TS, right: LFS, measured with divertor Langmuir probes.

amplitude. Small ELMs are regarded recently as having filamentary nature and filamentary transport is considered playing a crucial role in the density shoulder formation. Therefore variation in the density shoulder properties would have been expected due to such significant change in the filamentary transport. Hence, the unexpected result is investigated further: the same data are depicted again in figure 17, where two short time periods denoted with brown and yellow in figure 12 are plotted, now with estimated error bars. They show that the profiles are indistinguishable in the far SOL and the formation of a pedestal due to the L-H transition is also revealed. The reliability of the LiBES profiles drastically decreases inwards from the light profile peak which is at $\rho_p \approx 1.06$ in this case based on the bottom graph of the same figure. Hence, such good distinction between the L-mode and H-mode edge behaviour demonstrates, that the signal quality is excellent and the SOL observations should be trusted.

The limiter LP measurements neither show significant differences between L-mode and H-mode in figures 15(*e*) and (*f*). The 0.25 quantile can be regarded as an estimation of the n_e level of the background plasma and the mean is the average n_e level including background plasma and filaments. Their ratio is similar in L-mode and in H-mode, which also suggests that the role of small ELMs is small in the formation of the SOL n_e profiles.

5. Discussion

It was demonstrated in section 4 that the decreasing wall-separatrix distance increases the n_e levels locally when a density shoulder is present. A possible physical mechanism is discussed here. Additionally, it is put forward that the inconsistency among diagnostics can be attributed to the differences in the radial limiter-separatrix and in the absolute (and thus mainly toroidal) limiter-diagnostic distances at the same time.

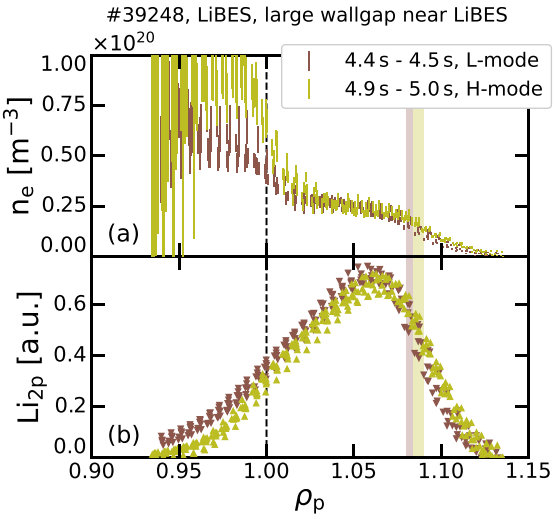


Figure 17. Electron density (*a*) and measured Li_{2p} emission (*b*) based on LiBES measurements around the midplane in L-mode (brown) and in H-mode (yellow) in #39248, when the wall gap was large near the LiBES. The vertical extensions of the markers in (*a*) correspond to profile and estimation uncertainties. Time ranges are denoted with corresponding colours in figure 12. Colourful vertical lines: limiter positions, dashed vertical black lines: separatrix position. The vertical lines are faded out for better visibility of the profiles.

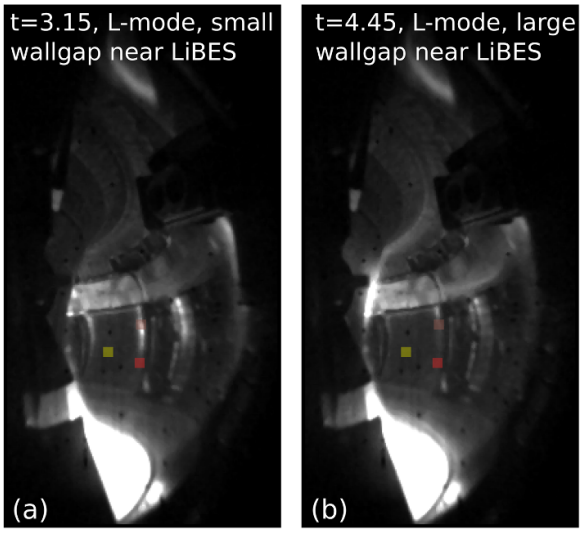


Figure 18. Images of a small (*a*) and a high (*b*) wall clearance plasma in #39248, where the SOL is limited on the top of the LFS ICRH antennae limiter near the LiBES. Fast visible camera measurement with H_α filter. Red and brown squares on the limiter: ROIs used in figure 15(*h*), when the background is taken from the yellow ROI.

5.1. Enhanced recycling around the limiters

Two photos recorded with the fast visible camera are shown in figure 18. They were taken in the L-mode parts of #39248 when the plasma was close to the the top of the ICRH antennae limiter (*a*) and far away from it (*b*). This feature appeared in the H_α radiation distribution: the region around the bottom of the ICRH limiter was always dark and the top was intensively radiating in (*a*). Regions of interest (ROIs) have been selected on the limiter, which are denoted by brown and red in the photos. They are around the same height as the LiBES and the HeBES respectively, although these two diagnostics are in different toroidal sectors. Additionally, the yellow square points to a location at the antennae region, where the emission is low. This is subtracted and the time traces are shown in figure 15(*h*). With this background correction, the contribution coming from the integration through the plasma is removed. The signals can be used only for qualitative investigation, since reflections from the wall can also significantly contribute to the intensities. The grey lines are the signals with the recorded $f = 2$ kHz temporal resolution and the dotted and solid lines correspond to the lower envelope (0.25 quantile) and to the mean value averaged over 20 ms, respectively.

If local recycling plays an important role governing n_e in the SOL the enhanced emission in the small wall clearance case (denoted by cyan patch in figure 15) could explain the deviation between the HeBES and LiBES in figure 4, since the separatrix-limiter radial distance is much smaller for the LiBES. The change of n_e^{LiBES} in figure 13 due to the locally changing wall clearance could also be explained with the change in the emission around the top, i.e. with the time evolution of the brown line in figure 15(*h*). The highly fluctuating nature of the 2 kHz signals demonstrates that filaments are present, reach the limiter, and enhance H_α radiation. However, the small difference between the mean signal values and the 0.25 quantiles suggests that their direct impact is not the dominant contributor. This is also suggested by the fact that the appearance of small ELMs in H-mode did not increase the SOL n_e in figure 17.

5.2. Differences in limiter-diagnostic distances

The camera images in figure 18 can demonstrate the difference in the H_α radiation levels between the poloidal locations of LiBES and HeBES. Hence, they corroborate that recycling is more intense around the LiBES, in line with the smaller limiter-separatrix radial distance. However, this explanation cannot be used for the MEM, since it is at nearly the same poloidal position as the LiBES and thus the separatrix-limiter radial distances are similar at around these two latter diagnostics. Hence, the other, namely the toroidal limiter-diagnostic distance is suspected to be responsible for that discrepancy. A photo is shown in figure 19, which was taken from the interior of ASDEX Upgrade during a recent opening. It shows, that the toroidal distance between the ICRH limiter and the LiBES is 11 cm and the toroidal distance between the MEM and the same limiter is 1.05 m, i.e approximately 10 times bigger than that. Although there is a guard limiter close to the MEM, it is retracted radially by 2 cm and the toroidal distance between this guard limiter and the MEM is 27 cm, i.e. approximately 2.5 times larger than the distance between

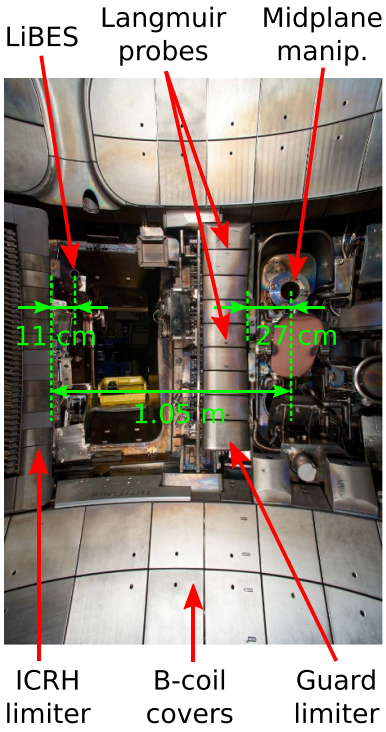


Figure 19. Photo of ASDEX Upgrade at around the LFS midplane taken during an opening. Toroidal distances are displayed.

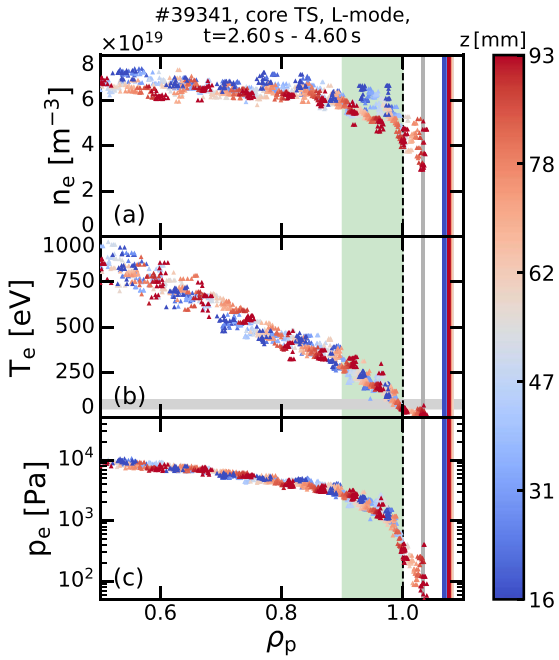


Figure 20. Electron density (*a*), temperature (*b*) and pressure (*c*) profiles halfway between the midplane and the X-point measured with the core TS diagnostic during the L-mode strike point scan in #39341. Colour code: plasma axis height. Vertical grey lines: end of outer divertor, colourful vertical lines: limiter positions, dashed vertical black lines: separatrix position. Vertical green patch: $\rho_p = 0.9 - 1$ spatial range, where change in n_e with stationary T_e is observed. Horizontal grey patch in (*b*): $T_e = 50\,\text{eV} - 100\,\text{eV}$ range, i.e. the possible range of the upstream separatrix temperature.

the ICRH limiter and the LiBES. So the higher toroidal (absolute) limiter-diagnostic distance in case of the MEM is also in line with the lower measured n_e.

5.3. Effect of wall proximity on the density of the plasma edge

The effect of the strike point scan was discussed in section 4.1 only at the midplane and in the divertor. Regrettably no diagnostic is available in the SOL during the entire scan around the location, where the plasma-wall distance was changing locally. Although the core TS is in that region, it has only one observation channel in the SOL and only in the second half of the plasma movement. However, the system can be used to study the effect of local wall clearance on the n_e profiles in the confined region, since it can reach the L-mode deep edge and the H-mode pedestal top regions, which can hardly be investigated by the edge TS, LiBES and HeBES diagnostics.

The profiles measured with the core TS are depicted in figure 20. The colour coding shows the vertical position of the plasma similarly to section 4.1. High $n_e^{\text{coreTh}} \approx 3.7 \cdot 10^{19}\,\text{m}^{-3}$ is measured in the far SOL. This value is closer to $n_e^{\text{LiBES}} \approx 3.1 \cdot 10^{19}\,\text{m}^{-3}$ than to $n_e^{\text{HeBES}} \approx 1.5 \cdot 10^{19}\,\text{m}^{-3}$, similarly to figure 4. The reason why the core TS measures higher n_e than the HeBES does in the far SOL in spite of the higher wall-separatrix radial distance around the core TS may be dual: the tiles above the B-coils cover the vacuum vessel toroidally symmetrically in this region, as shown in figure 19. Hence, the wall surface close to the observation location is much larger in the core TS case. The other contribution to the enhancement can come from the proximity of the divertor based on the 2-point model [35], since the connection length to the X-point is only $L_c^{\text{X-point}} \approx 3 - 4\,\text{m}$, which is shorter than to the midplane $L_c^{\text{midplane}} \approx 6 - 7\,\text{m}$.

The deep edge, i.e. the $\rho_p = 0.9 - 1$ range is denoted by a light green patch in figure 20. The core TS had coverage during the entire discharge here. The T_e profiles stayed stationary during the scan, but the n_e profiles were evolving. When the wall gap was high (red case, at the end of the scan) the profiles were smoothly decreasing outwards. When the plasma was locally close to the wall (blue case, at the beginning of the scan) n_e was higher at the edge and the profiles were flat. An even stronger enhancement of n_e has been measured in H-mode (not shown here), where a peak also appeared at the pedestal top. Similar observation has not been done with the LiBES, HeBES and edge TS diagnostics, but this could also be related to the fact, that these systems are not optimal to measure there. The O-mode reflectometer, which would be suitable to study the plasma edge, was not in operation. However, discrepancy between the core TS and this reflectometer is a known issue there [47], which might also suggest that n_e is only locally increased in the core TS region. As can be seen in figure 9 the behaviour of the HFSHD was the opposite to the edge: n_e was increasing there simultaneously to the increasing wall gap and thus to the decreasing edge n_e.

It is not expected that the profiles are strictly flux functions in the confined region. As an example the GRILLIX high collisionality run [48] shows enhanced n_e in the X-point region even without recycling wall when X-point radiator [49] is not present. Including the wall in that code is regarded as long-term strategy to justify the effect of the recycling wall on the main plasma.

6. Conclusions

A possible mechanism that controls the n_e levels in the far SOL has been investigated experimentally. The study started with introducing an experimental finding: the SOL diagnostics at ASDEX Upgrade provide consistent data before the density shoulder formation and they start to deviate as the profiles start to flatten. At high SOL n_e this discrepancy can reach up to factor of 3. A hypothesis has been postulated that the deviation originates from the differences in the wall-separatrix and in the wall-diagnostic distances.

The experiments to test the idea focused on locally changing the wall-separatrix radial distance. They were carried out in a plasma regime after the H-L back transition, when the SOL profiles were flat up to the flux surface of the deepest immersed limiter, and the typical plasma parameters were $n_e \approx 2-4\cdot 10^{19}\,\mathrm{m}^{-3}$ and $T_e \approx 15\,\mathrm{eV}$ in the far SOL. This plasma region was investigated with several diagnostics in the scrape-off layer. When the local wall clearance was increased from 4 cm to 7 cm n_e decreased at the midplane. However, the increase of wall gap at the bottom part of the plasma with the so-called strike point scan had no influence on the midplane profiles, in line with the importance of local wall-separatrix distance. The effect can be a significant contribution to the elevated n_e^{LiBES} relative to n_e^{HeBES}: the wall gap was only 4 cm around the LiBES and 75 percent higher around the HeBES in the investigated case.

Since the LiBES and the MEM are situated at the same poloidal position the inconsistency between their measurement results can be related to the different absolute distances of the diagnostics to the wall. The toroidal and thus the absolute distance between the LiBES and the main ICRH limiter is only 10 cm and the MEM is almost twice as far from a retracted guard limiter and 10 times further away from a main ICRH limiter toroidally. Hence, the factor of 2 increase in n_e can be attributed to the wall proximity in the LiBES case.

Recycling is a physical process that is enhanced when the wall-separatrix distance is small and could increase n_e.

Interestingly, the effect of a strike point scan is observed on the local edge profiles, too. This is interpreted similarly as above: the wall proximity enhances n_e even at the edge top (or at the pedestal top in H-mode), which can result in locally flat or non-monotonic profiles.

Some experiments were carried out in QCE H-mode, but this change in the plasma regime neither influenced the processes nor the n_e levels in the SOL. Hence, small ELMs may not be the key contributors to the SOL n_e.

In summary, the study concludes that n_e is highly influenced by the distance between the separatrix and the local wall elements in the scrape-off layer, if a density shoulder is formed. Hence, toroidal SOL symmetry can only be assumed when the first wall is also toroidally symmetric, which is the case neither on ASDEX Upgrade nor on ITER. The experimental investigation of the phenomenon is challenging, since the measurement results depend on the measurement locations relative to the wall. The presented experimental findings in ASDEX Upgrade should be taken into account in studies where local measurements are used to calculate the total wall exposure. While such an extrapolation might be valid at low densities, at high densities the shown asymmetries can lead to large errors. As a next step, 3D modelling will have to confirm the findings and explain the physical processes that create the asymmetries. Such a validation exercise will strengthen our capability of predicting wall loads in future fusion devices. Thus, 3D modelling that includes recycling from first wall elements will play a key role in future studies.

Acknowledgment

This work has been carried out within the framework of the EUROfusion Consortium, funded by the European Union via the Euratom Research and Training Programme (Grant Agreement No. 101052200 - EUROfusion). Views and opinions expressed are however those of the authors only and do not necessarily reflect those of the European Union or the European Commission. Neither the European Union nor the European Commission can be held responsible for them.

Appendix. Effect of filament activity on the LiBES density profiles

Typically the LiBES diagnostic provides the highest n_e values at the midplane when a density shoulder is formed and thus inconsistency among n_e measurements is experienced. This plasma state always has a highly filamentary nature, which results in fluctuating nonmonotonic profiles in the SOL on a below 1 kHz timescale. Since the n_e calculation method [21] assumes weak monotonicity inwards, the question arose whether this constraint made the code flatten the holes between the filaments and the pedestal and thus overestimate n_e. A numerical test is introduced in this appendix to demonstrate that this is not the case, i.e. n_e measured with the LiBES in figure 4 is higher than other measurements not due to overestimation of n_e.

The test method is explained in figure A1. Artificial but realistic filamentary n_e profiles are created and shown in (a), then synthetic LiBES signals are calculated from these modified profiles with the SIMULA code [50], which is based on a collisional-radiative model. They are depicted in (b). Then n_e profiles are reconstructed from the synthetic light profiles with the IDA code, which is otherwise used to determine n_e profiles from measurement data. They are shown in (c). The comparison between the input and the reconstructed profiles determines, how much the inversion method is biased.

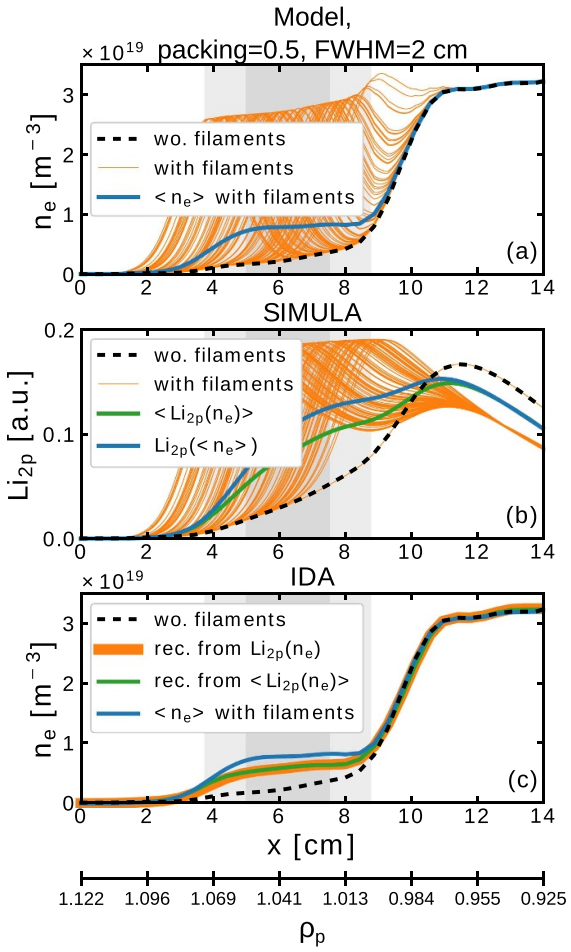


Figure A1. (a) n_e used as input to test LiBES reconstructions—orange curves. (*b*) Synthetic light profiles calculated from (*a*). (*c*) Single n_e profile reconstructed from the many orange light profiles in (*b*) and from the single green light profile in (*b*). x is the spatial coordinate along the Li beam. As second horizontal axis the ρ_p of the 'wo. filaments' case (#38910 at $t = 5.4$ s) is depicted. Light grey patch: region where filament center locations are uniformly distributed. Dark grey patch: region where average n_e is calculated for figure A2.

A typical exponentially decaying profile in an interELM H-mode phase is selected (in #38910 at $t = 5.4$ s [51]) and Gaussian-shaped perturbations are added to it to get the artificial profiles. FWHM $= 2$ cm [52] is applied as width and $A = 2.5 \cdot 10^{19}$ m^{-3} as amplitude, which is almost as big as the height of the pedestal in this case. They are shown in figure A1(*a*) with orange lines. Here the spatial coordinate corresponds to a distance along the Li beam, i.e. approximately radially inward at $z = 0.326$ m height. The centre of the filaments are chosen randomly in the $x = 3.75$ cm $-$ 8.75 cm range shown by a light grey patch in the figure. 200 profiles are created in total, in correspondence with the applied 50 μs sampling time and 10 ms profile time used in this study. Half of the profiles contain filament perturbation, which is described as a packing fraction of 0.5. No correlation is applied among the profiles. Their average is shown in (a) with blue. The original profile can also be recognized here as the lower envelope of the orange lines.

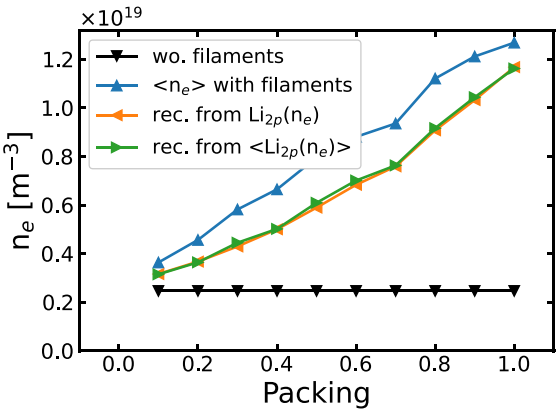


Figure A2. Model and from the model reconstructed average n_e in the shoulder region (depicted by a dark grey patch in this figure) as a function of filament packing fraction.

The synthetic light profiles are depicted in figure A1(*b*). The orange lines here are individual calculations from the orange n_e profiles in (*a*). If this was a real experiment they would correspond to the measurement data. Their average is shown in (b) by green. Additionally, a blue curve is also depicted here, which is the synthetic light profile of the average n_e. This could not be obtained in a real experiment, since the average n_e profile is never present.

n_e profiles are shown again in figure A1(*c*). Two curves are identical here to (a): the black curve is the reference without filaments—this is the lower envelope of the orange profiles in (a) - and the blue curve is the average n_e. Similarly to (b) it would not be possible to obtain this latter one in real experiments. The result of the reconstruction coming from the average of the light profiles is depicted by green and the one calculated from the 200 individual light profiles is depicted by orange.

In figure A1 both the orange and green profiles could be calculated from experimental data, too. The agreement between them just states that the result is indifferent to this adjustment in the reconstruction code among these circumstances. The reconstructed curves (orange and green curves) are below the real average (blue curve). The underestimation suggests that the real n_e can be even higher at the LiBES location in figure 4, i.e. the inconsistency cannot originate from the estimation method. This behaviour is the opposite than was expected from the monotonicity constraint. It does not come from the reconstruction but it is already in the collisional-radiative model: figure A1(*b*) shows that the average of the light profiles (green curve) is lower in the vicinity of the filaments than the light profile coming from the average (blue curve). This might come from the realistic assumption that recombination is not possible in this system. Hence, the enhanced ionisation frequency due to higher n_e in the filament is not compensated in the low n_e region between the filament and the pedestal.

To further prove that n_e is slightly underestimated when filaments are present the numerical test is repeated with varying the packing fraction, i.e. the significance of the filament activity. The results are summarized in figure A2. Here n_e is calculated as the average in the $x = 5$ cm $-$ 7.5 cm range, which is

denoted with a dark grey patch in figure A1. The colours have similar meaning in both figures. The slight difference between the blue and the orange (or green) curves in the latter figure justifies that n_e is always slightly underestimated, although the level of bias depends slightly on the filament frequency.

ORCID iDs

B. Tal https://orcid.org/0009-0009-5316-6358
E. Wolfrum https://orcid.org/0000-0002-6645-6882
M. Bernert https://orcid.org/0000-0003-1131-0867
G. Birkenmeier https://orcid.org/0000-0001-7508-3646
D. Brida https://orcid.org/0000-0002-8647-7058
R. Fischer https://orcid.org/0009-0000-6205-4731
G. Grenfell https://orcid.org/0000-0003-0107-5787
M. Griener https://orcid.org/0000-0003-2953-536X
O. Grover https://orcid.org/0000-0002-7695-8050
J. Hobirk https://orcid.org/0000-0001-6605-0068
B. Kurzan https://orcid.org/0000-0002-2683-9635
T. Lunt https://orcid.org/0000-0002-7386-1456
P.A. Schneider https://orcid.org/0000-0001-7257-3412
N. Vianello https://orcid.org/0000-0003-4401-5346
D. Wendler https://orcid.org/0000-0002-8838-0137

References

[1] Bernert M. *et al* (the ASDEX Upgrade Team) 2014 The H-mode density limit in the full tungsten ASDEX Upgrade tokamak *Plasma Phys. Control. Fusion* **57** 014038
[2] McCormick K., Kyriakakis G., Neuhauser J., Kakoulidis E., Schweinzer J. and Tsois N. 1992 Particle and energy transport scalings in the ASDEX scrape-off layer *J. Nucl. Mater.* **196–198** 264–70
[3] Asakura N., Koide Y., Itami K., Hosogane N., Shimizu K., Tsuji-Iio S., Sakurai S. and Sakasai A. 1997 SOL plasma profiles under radiative and detached divertor conditions in JT-60U *J. Nucl. Mater.* **241–243** 559–63
[4] LaBombard B., Boivin R.L., Greenwald M., Hughes J., Lipschultz B., Mossessian D., Pitcher C.S., Terry J.L. and Zweben S.J. (the Alcator Group) 2001 Particle transport in the scrape-off layer and its relationship to discharge density limit in Alcator C-Mod *Phys. Plasmas* **8** 2107–17
[5] Rudakov D. *et al* 2005 Far SOL transport and main wall plasma interaction in DIII-D *Nucl. Fusion* **45** 1589
[6] Garcia O., Pitts R., Horacek J., Nielsen A., Fundamenski W., Graves J., Naulin V. and Rasmussen J.J. 2007 Turbulent transport in the TCV SOL *J. Nucl. Mater.* **363-365** 575–80
[7] Carralero D., Birkenmeier G., Müller H., Manz P., deMarne P., Müller S., Reimold F., Stroth U., Wischmeier M. and Wolfrum E. (the ASDEX Upgrade Team) 2014 An experimental investigation of the high density transition of the scrape-off layer transport in ASDEX Upgrade *Nucl. Fusion* **54** 123005
[8] Militello F., Garzotti L., Harrison J., Omotani J., Scannell R., Allan S., Kirk A., Lupelli I. and Thornton A. (the MAST Team) 2015 Characterisation of the L-mode scrape off layer in MAST: decay lengths *Nucl. Fusion* **56** 016006
[9] Wynn A. *et al* (the JET Contributors) 2018 Investigation into the formation of the scrape-off layer density shoulder in JET ITER-like wall L-mode and H-mode plasmas *Nucl. Fusion* **58** 056001
[10] Yan N. *et al* 2021 Dependence of upstream SOL density shoulder on divertor neutral pressure observed in L-mode and H-mode plasmas in the EAST superconducting tokamak *Nucl. Fusion* **61** 076018
[11] Carralero D. *et al* (the ASDEX Upgrade Team, the COMPASS Team and the JET-EFDA Contributors) 2015 Implications of high density operation on SOL transport: A multimachine investigation *J. Nucl. Mater.* **463** 123–7
[12] Vianello N. *et al* (the ASDEX Upgrade Team, the TCV Team and the EUROfusion MST1 Team) 2019 Scrape-off layer transport and filament characteristics in high-density tokamak regimes *Nucl. Fusion* **60** 016001
[13] Carralero D., Manz P., Aho-Mantila L., Birkenmeier G., Brix M., Groth M., Müller H.W., Stroth U., Vianello N. and Wolfrum E. (the ASDEX Upgrade Team, the JET Contributors and the EUROfusion MST1 Team) 2015 Experimental Validation of a Filament Transport Model in Turbulent Magnetized Plasmas *Phys. Rev. Lett.* **115** 215002
[14] Carralero D. *et al* (the EUROfusion MST1 Team and the ASDEX Upgrade Team) 2017 A study on the density shoulder formation in the SOL of H-mode plasmas *Nucl. Mater. Energy* **12** 1189–93
[15] Stagni A. *et al* (the TCV Team and the EUROfusion MST1 Team) 2022 Dependence of scrape-off layer profiles and turbulence on gas fuelling in high density H-mode regimes in TCV *Nucl. Fusion* **62** 096031
[16] Redl A., Eich T., Vianello N. and David P. (the ASDEX Upgrade Team and the EUROfusion MST1 Team) 2023 Energy load on first wall components in high density, small ELM regimes in ASDEX Upgrade *Nucl. Mater. Energy* **34** 101319
[17] Tsui C.K. *et al* (the TCV Team and the EUROfusion MST1 Team) 2022 Evidence on the effects of main-chamber neutrals on density shoulder broadening *Phys. Plasmas* **29** 062507
[18] Carralero D., Artene S., Bernert M., Birkenmeier G., Faitsch M., Manz P., de Marne P., Stroth U., Wischmeier M. and Wolfrum E. (the ASDEX Upgrade Team and the EUROfusion MST1 Team) 2018 On the role of filaments in perpendicular heat transport at the scrape-off layer *Nucl. Fusion* **58** 096015
[19] Bock L., Brida D., Faitsch M., Schmid K. and Lunt T. (the ASDEX Upgrade Team) 2021 Comparison of the influence of 2D and 3D geometry of the main chamber on plasma parameters in the SOL of ASDEX Upgrade *Nucl. Fusion* **62** 026020
[20] Willensdorfer M., Birkenmeier G., Fischer R., Laggner F.M., Wolfrum E., Veres G., Aumayr F., Carralero D., Guimarãis L. and Kurzan B. (the ASDEX Upgrade Team) 2014 Characterization of the Li-BES at ASDEX Upgrade *Plasma Phys. Control. Fusion* **56** 025008
[21] Fischer R., Wolfrum E. and Schweinzer J. (the ASDEX Upgrade Team) 2008 Probabilistic lithium beam data analysis *Plasma Phys. Control. Fusion* **50** 085009
[22] Grenfell G. *et al* (the ASDEX Upgrade Team) 2022 High-heat flux ball-pen probe head in ASDEX-Upgrade *Rev. Sci. Instrum.* **93** 023507
[23] Griener M., Wolfrum E., Cavedon M., Dux R., Rohde V., Sochor M., Muñoz Burgos J.M., Schmitz O. and Stroth U. (the ASDEX Upgrade Team) 2018 Helium line ratio spectroscopy for high spatiotemporal resolution plasma edge profile measurements at ASDEX Upgrade (invited) *Rev. Sci. Instrum.* **89** 10D102
[24] Griener M. *et al* (the ASDEX Upgrade Team) 2017 Qualification and implementation of line ratio spectroscopy on helium as plasma edge diagnostic at ASDEX Upgrade *Plasma Phys. Control. Fusion* **60** 025008
[25] Wendler D., Dux R., Fischer R., Griener M., Wolfrum E., Birkenmeier G. and Stroth U. (the ASDEX Upgrade Team) 2022 Collisional radiative model for the evaluation of the

thermal helium beam diagnostic at ASDEX upgrade *Plasma Phys. Control. Fusion* **64** 045004
[26] Nishizawa T., Griener M., Dux R., Grenfell G., Wendler D., Kado S., Manz P. and Cavedon M. (the ASDEX Upgrade Team) 2021 Linearized spectrum correlation analysis for thermal helium beam diagnostics *Rev. Sci. Instrum.* **92** 103501
[27] Griener M., Kalis J., Wendler D., Birkenmeier G., Wolfrum E., McDermott R., Stroth U. and Team A.U. (the ASDEX Upgrade Team and the EUROfusion MST1 Team) 2023 Compensation of plasma fluctuation induced shadowing effects in gas puff imaging data *Nucl. Mater. Energy* **34** 101346
[28] Wendler D., Birkenmeier G., Griener M., Dux R., Fischer R., Stieglitz D., Wolfrum E. and Stroth U. (the ASDEX Upgrade Team) 2023 Two-dimensional reconstruction of filament temperatures and densities with the thermal helium beam at ASDEX Upgrade *Phys. Plasmas* **30** 092509
[29] Griener M. *et al* (the ASDEX Upgrade Team) 2017 Fast piezoelectric valve offering controlled gas injection in magnetically confined fusion plasmas for diagnostic and fuelling purposes *Rev. Sci. Instrum.* **88** 033509
[30] Kurzan B. and Murmann H.D. 2011 Edge and core Thomson scattering systems and their calibration on the ASDEX Upgrade tokamak *Rev. Sci. Instrum.* **82** 103501
[31] Kurzan B., Jakobi M. and Murmann H. (the ASDEX Upgrade Team) 2003 Signal processing of Thomson scattering data in a noisy environment in ASDEX Upgrade *Plasma Phys. Control. Fusion* **46** 299
[32] Kurzan B. 2024 private communication
[33] Fischer R. *et al* (the ASDEX Upgrade Team) 2016 Coupling of the Flux Diffusion Equation with the Equilibrium Reconstruction at ASDEX Upgrade *Fusion Sci. Technol.* **69** 526–36
[34] Fischer R., Fuchs C.J., Kurzan B., Suttrop W. and Wolfrum E. (the ASDEX Upgrade Team) 2010 Integrated Data Analysis of Profile Diagnostics at ASDEX Upgrade *Fusion Sci. Technol.* **58** 675–84
[35] Pitcher C.S. and Stangeby P.C. 1997 Experimental divertor physics *Plasma Phys. Control. Fusion* **39** 779
[36] Illerhaus J. 2018 Estimation, validation and uncertainty of the position of the separatrix contour at ASDEX Upgrade *Master's Thesis* Technische Universitaet Muenchen
[37] Cavedon M. *et al* (the ASDEX Upgrade Team) 2022 Experimental investigation of L- and H-mode detachment via the divertor Thomson scattering at ASDEX Upgrade *Nucl. Fusion* **62** 066027
[38] Lunt T. *et al* (the ASDEX Upgrade Team) 2020 Near- and far scrape-off layer transport studies in detached, small-ELM ASDEX Upgrade discharges by means of EMC3-EIRENE *Plasma Phys. Control. Fusion* **62** 105016
[39] Mlynek A., Schramm G., Eixenberger H., Sips G., McCormick K., Zilker M., Behler K. and Eheberg J. (the ASDEX Upgrade Team) 2010 Design of a digital multiradian phase detector and its application in fusion plasma interferometry *Rev. Sci. Instrum.* **81** 033507
[40] Greenwald M., Terry J., Wolfe S., Ejima S., Bell M., Kaye S. and Neilson G. 1988 A new look at density limits in tokamaks *Nucl. Fusion* **28** 2199
[41] Yang Z., Krieger K., Lunt T., Brochard F., Briancon J.-L., Neu R., Dux R., Janzer A., Potzel S. and Pütterich T. (the ASDEX Upgrade Team) 2013 3D trajectories re-construction of droplets ejected in controlled tungsten melting studies in ASDEX Upgrade *J. Nucl. Mater.* **438** S846–51
[42] Carralero D. *et al* (the ASDEX Upgrade Team, the COMPASS Team, the JET Contributors and the EUROfusion MST1 Team) 2017 Recent progress towards a quantitative description of filamentary SOL transport *Nucl. Fusion* **57** 056044
[43] Reimold F., Wischmeier M., Bernert M., Potzel S., Kallenbach A., Müller H., Sieglin B. and Stroth U. (the ASDEX Upgrade Team) 2015 Divertor studies in nitrogen induced completely detached H-modes in full tungsten ASDEX Upgrade *Nucl. Fusion* **55** 033004
[44] Kallenbach A. *et al* (the ASDEX Upgrade Team) 2015 Partial detachment of high power discharges in ASDEX Upgrade *Nucl. Fusion* **55** 053026
[45] Faitsch M., Eich T., Harrer G., Wolfrum E., Brida D., David P., Griener M. and Stroth U. (the ASDEX Upgrade Team and the EUROfusion MST1 Team) 2021 Broadening of the power fall-off length in a high density, high confinement H-mode regime in ASDEX Upgrade *Nucl. Mater. Energy* **26** 100890
[46] Faitsch M., Eich T., Harrer G., Wolfrum E., Brida D., David P., Dunne M., Gil L., Labit B. and Stroth U. (the ASDEX Upgrade Team and the EUROfusion MST1 Team) 2023 Analysis and expansion of the quasi-continuous exhaust (QCE) regime in ASDEX Upgrade *Nucl. Fusion* **63** 076013
[47] Stieglitz D.J., Santos J. and Fischer R. (the ASDEX Upgrade Team) 2023 Implementation and validation of swept density reflectometry for integrated data analysis at ASDEX Upgrade *Rev. Sci. Instrum.* **94** 043503
[48] Zholobenko W., Pfennig J., Stegmeir A., Body T., Ulbl P. and Jenko F. (the ASDEX Upgrade Team) 2023 Filamentary transport in global edge-SOL simulations of ASDEX Upgrade *Nucl. Mater. Energy* **34** 101351
[49] Bernert M. *et al* (the EUROfusion MST1 Team and the ASDEX Upgrade Team) 2020 X-point radiation, its control and an ELM suppressed radiating regime at the ASDEX Upgrade tokamak *Nucl. Fusion* **61** 024001
[50] Schweinzer J., Wolfrum E., Aumayr F., Pockl M., Winter H., Schorn R.P., Hintz E. and Unterreiter A. 1992 Reconstruction of plasma edge density profiles from Li I (2s-2p) emission profiles *Plasma Phys. Control. Fusion* **34** 1173
[51] Bock A. *et al* (the ASDEX Upgrade Team) 2017 Non-inductive improved H-mode operation at ASDEX Upgrade *Nucl. Fusion* **57** 126041
[52] Birkenmeier G. *et al* (the ASDEX Upgrade Team) 2014 Magnetic field dependence of the blob dynamics in the edge of ASDEX upgrade L-mode plasmas *Plasma Phys. Control. Fusion* **56** 075019